TITLE

Convergent human and climate forcing of late-Holocene flooding in northwest England

AUTHORS

Schillereff, D.N.[1], Chiverrell, R.C.[2], Macdonald, N.[2], Hooke, J.M.[2], Welsh, K.E.[3], Piliposian, G.[4], Croudace, I.W.[5]

[1]Department of Geography, King's College London, London, UK
[2]School of Environmental Sciences, Roxby Building, University of Liverpool, Liverpool, UK
[3]Department of Geography and International Development, University of Chester, Chester, UK
[4]Department of Mathematical Sciences, Environmental Radioactivity Research Centre, University of Liverpool, Liverpool, UK
[5]GAU-Radioanalytical, University of Southampton, National Oceanography Centre, Southampton, UK

ABSTRACT

Concern is growing that climate change may amplify global flood risk but short hydrological data series hamper hazard assessment. Lake sediment reconstructions are capturing a fuller picture of rare, high-magnitude events but the UK has produced few lake palaeoflood records. We report the longest lake-derived flood reconstruction for the UK to date, a 1500-year record from Brotherswater, northwest England. Its catchment is well-suited physiographically to palaeoflood research, but its homogeneous, dark brown sediment matrix precludes visual identification of flood layers. Instead, an outlier detection routine applied to high-resolution particle size measurements showed a >90% match, in stratigraphic sequence, to measured high river flows. Our late-Holocene palaeoflood reconstruction reveals nine multi-decadal periods of more frequent flooding (CE 510-630, 890-960, 990-1080, 1470-1560, 1590-1620, 1650-1710, 1740-1770, 1830-1890 and 1920-2012), and these show a significant association with negative winter North Atlantic Oscillation (wNAO) phasing and some synchrony with solar minima. These flood-rich episodes also overlap with local and regional land-use intensification, which we propose has amplified the flood signal by creating a more efficient catchment sediment conveyor and more rapid hillslope-channel hydrological connectivity. Disentangling anthropogenic and climatic drivers is a challenge but anthropogenic landscape transformation should evidently not be underestimated in palaeoflood reconstructions. Our paper also demonstrates that flood histories can be extracted from the numerous lakes worldwide containing organic-rich, visually homogeneous sediments. This transformative

evidence base should lead to more reliable assessments of flood frequency and risks to ecosystems and infrastructure.

KEY WORDS

Flood hazard; Human activity; Lake sediments; North Atlantic Oscillation; Paleofloods; Solar forcing

1. INTRODUCTION

Flooding accounted for 39% of global natural disasters between 2000 and 2016, with severe social and economic consequences (CRED, 2018). Growing concern that climate change is amplifying hazards from river flooding (Blöschl et al., 2017; Otto et al., 2018) has directed a focus on the uncertainties attached to the most extreme and inherently rare events (Kjeldsen and Prosdocimi, 2018). Flood frequency calculations—usually reported as return periods—are conventionally derived from instrumental river flow data (Institute of Hydrology, 1999). Unfortunately, the operational lifespan of river gauging stations (~40 years in the UK; Hannaford, 2015) is rarely of sufficient duration to capture the full range of hydrological variability. Pooling methods that incorporate regional data can augment flood frequency analysis (Miller et al., 2013; Reed and Robson, 1999) but short time series are a persistent obstacle when calculating return periods of rare, high-magnitude floods (Macdonald and Sangster, 2017). As a result, non-conventional sources of flood data that extend beyond the instrumental record are increasingly sought (Lam et al., 2017).

Alongside documentary records (Kjeldsen et al., 2014; Parkes and Demeritt, 2016), botanical indicators (Wilhelm et al., 2018b), speleothems (Denniston and Luetscher, 2017) and alluvial deposits (Munoz et al., 2018), there has been a growing focus on lake sediments as a palaeoflood archive (Gilli et al., 2013; Schillereff et al., 2014; Wilhelm et al., 2018a). Under favourable catchment and lake basin physiographic conditions, a signal of the catchment sediment cascade preserved at a lake bed can be sensitive to variations in river discharge, yielding event-scale palaeoflood records spanning centuries or millennia (e.g., Chiverrell et al., 2019; Czymzik et al., 2013; Vasskog et al., 2011; Wilhelm et al., 2013; Wirth et al., 2013a). Certain lakes with optimal basin configurations reveal annually- or seasonally resolved stratigraphies, from which flood deposits can be clearly differentiated and attributed to a single year or season (Amann et al., 2015; Kämpf et al., 2014; Wirth et al., 2013a). Few palaeoflood reconstructions have emerged, however, from the scores of lakes worldwide that accumulate dark-brown, organic-rich, homogeneous sediment matrices (Pennington, 1991). Visual detection of flood laminations is a major challenge in these lakes. Moreover, their drainage basins have widely been subjected to anthropogenic landscape modification through the

Holocene, given they are commonly located in more lowland settings (Edwards and Whittington, 2001). Such perturbations to the catchment-to-lake sediment conveyor may blur the link between high discharges and their sedimentological and geomorphological effects through time (Hooke, 2015). The UK, in particular, has many such lakes but lags behind other parts of the world in the use of lake sediments as a palaeoflood archive.

We report a >1500-year palaeoflood record from Brotherswater, a lake in the headwaters of the flood-prone Eden Catchment, northwest England (Macdonald and Sangster, 2017; Parkes and Demeritt, 2016; Pattison and Lane, 2012). This is the longest lake-derived flood reconstruction to date for the UK. Schillereff et al. (2016a) revealed basin controls on contemporary sediment flux to Brotherswater result in signatures of recent floods being preserved as variation in particle size deposition. The sequence of storms that swept across northern Britain in winter 2015/16 delivered unprecedented levels of rainfall and triggered severe flooding (Burt et al., 2016; Marsh et al., 2016). Floods in 2005 (Environment Agency, 2006) and 2009 (Eden and Burt, 2010; Miller et al., 2013; Sibley, 2009) had similar-scale impacts and pooled peak flow return periods for the River Eamont (downstream of Brotherswater) were revised downwards by an order of magnitude (5877 to 460 years; Miller et al. 2013). Re-assessment after Storm Desmond (December 2015) further reduced this estimate to 350 years (Spencer et al., 2017). Longer hydrological time series that capture greater numbers of extreme floods are clearly needed to contextualise regional flood frequency estimates.

The Brotherswater palaeoflood record provides an important test of the viability of extracting flood data from these homogeneous sediment sequences and their fidelity when evaluated against independent river flow data. This record should also shed new light on long-term climate forcings that propagate westerlies from the North Atlantic. These storm tracks are responsible for most recent floods in the UK and western Europe (De Luca et al., 2017). Situated in a region with a long history of anthropogenic impacts (Chiverrell, 2006; Pennington, 1991; Winchester, 1987), the paper also aims to disentangle the influence of land-use change on palaeohydrological dynamics via parallel sedimentological and geochemical analysis.

2. REGIONAL SETTING

2.1 *Regional hydroclimate*

Meteorological patterns in northwest England are largely driven by moisture-laden westerly zonal air masses, owing to the maritime setting (Burt and Ferranti, 2012). Westerly and south-westerly cyclonic systems have been linked to regional 21st-century floods (Spencer et al., 2017) and earlier historical extreme events (Pattison and Lane, 2012) and their formation appears correlated with the winter North Atlantic Oscillation (wNAO) Index (Jones et al., 1997;

Wilby et al., 1997). The NAO appears to exert some control over the timing and duration of regional wet phases (Fowler and Kilsby, 2002; Pattison and Lane, 2012) but linkages between both positive and negative NAO phases and high flows in Britain (Foulds and Macklin, 2016; Hannaford and Marsh, 2008) emphasise its complexity as a flood generating mechanism. Similarly, the statistical link between flood frequency and multi-decadal fluctuations in North Atlantic Sea Surface Temperatures (SSTs) driven by the Atlantic Multi-decadal Oscillation (AMO) varies spatially across the UK and temporally over the last three centuries (Macdonald and Sangster, 2017). There is good evidence that solar forcing drives Holocene flooding in western Europe (Moreno et al., 2008) and the European Alps (Czymzik et al., 2016; Wilhelm et al., 2012; Wirth et al., 2013b) through ocean-atmosphere interactions in the North Atlantic, whereas links between solar activity and wet/dry periods recorded in UK peat sequences is rather more equivocal (Charman et al., 2006). Macdonald and Sangster (2017) advocate developing longer palaeoflood records that extend beyond documentary sources to help untangle such complexity.

2.2 *Field site*

Brotherswater is a small, mesotrophic lake located in the eastern Lake District National Park, northwest England (54.5066°N, 2.9249°W; 158 m above sea level) (Figures 1A-D). The physical characteristics of the lake basin and its catchment meet many criteria conducive to the preservation of palaeoflood records (Schillereff et al., 2014). The high catchment area (13.01 km^2) to lake surface area (0.18 km^2) ratio (72:1) ensures ample and continuous sediment availability (Semertzidou et al. 2019) for the preservation of deposits lain down under flood conditions (Schillereff et al., 2016a). Further, the deep, bowl-like basin with a flat, central abyssal zone has a maximum water depth of 16 m, which limits the potential for wind or wave-induced remobilisation of profundal sediments (Dearing, 1997). The visually homogeneous sediment matrix poses a challenge to discerning palaeoflood laminations, however (Chambers, 1978; Schillereff et al., 2016a).

Brotherswater lies in a glacial trough with steep catchment slopes formed by ice movement, most recently during Greenland Stadial 1 (McDougall, 2013). Catchment geology is dominated by Ordovician andesitic tuffs of the Borrowdale Volcanic Series, overlain by Pleistocene morainic and talus deposits on the lower slopes and valley floor. This paraglacial legacy (Ballantyne, 2002) yields a readily mobilised supply of sediment. Shallow (<30 cm), mineral-rich podzol and podzolic brown earth soils are found on lower slopes and thicker peaty soils cover higher ridges. Today, catchment forest cover has been almost entirely replaced by open sheep grazing and some improved pasture (Figure 1C), increasing the susceptibly of soils to erosion.

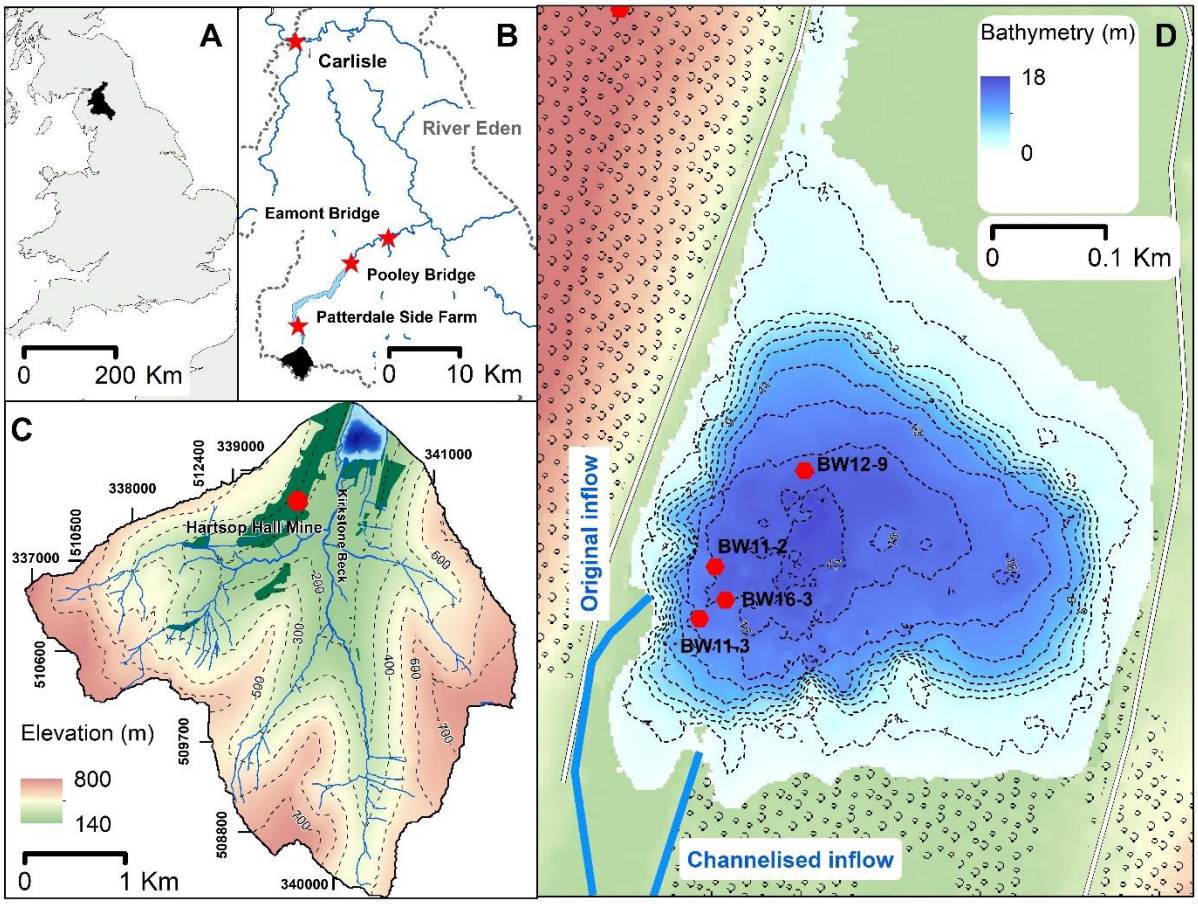

Figure 1. A) The River Eden drainage basin (black fill) in northwest England. **B)** The Brotherswater subcatchment (black fill) of the River Eden (grey dashes). River gauging stations used in this study (Patterdale, Pooley Bridge, Eamont Bridge) and the city of Carlisle are shown (red stars). Grisedale Bridge rain gauge is adjacent to Patterdale Side Farm. **C)**, Extent and topography of the Brotherswater catchment, showing the inflow and tributaries, Hartsop Hall Mine and woodland cover (dark green). **D)** Bathymetric map (2-m contours) of Brotherswater showing the four coring locations and the inflow position before and after manual diversion in the late-19th century.

Kirkstone Beck enters the lake at the southeast corner and is fed by five tributaries draining the upland headwaters (Figure 1C). Ordnance Survey maps from Common Era (CE) 1897 (OS, 2018a) show the inflow in the current position, whereas the 1861 product (OS, 2018b) shows the inflow ~50 metres to the west. Peak mining at Hartsop Hall Mine (Figure 1C) occurred between CE 1863 and 1871 (Tyler, 1992). The river was most likely diverted at this time to stabilise the western shoreline and allow mine access road construction. A sketch dated to CE 1794 confirms the inflow in the southwest corner, which we interpret as its long-

term position. Palaeochannels on the pre-lake floodplain and southern littoral waters point to previous inflow-delta configurations but cores from their toes suggests prolonged inactivity.

Mean annual precipitation (MAP) near Brotherswater is 2400 mm, with significant inter-annual variability. Minimum and maximum MAP, based on the incomplete but lengthy (since CE 1878) Grisedale Bridge record (Figure 1B), are 1600 and 3000 mm, respectively. The 2009 and 2015 floods, which had major impacts across the Lake District (Spencer et al., 2017), were produced by 24-hour rainfall volumes of 153.4 and 245 mm. The previous daily maximum rainfall was 138.7 mm on 10 October 1977. River flow data from Eamont Bridge (Figure 1B) show all major floods since CE 1962 occurred between October and March, so our palaeoflood reconstruction most likely documents winter floods, although summer convective storms cannot be ruled out.

3. METHODS

3.1 *Core acquisition and logging*

Lake bathymetry was determined using a Garmin 50/200 kHz dual frequency echo-sounder. Total lead (Pb) profiles measured by X-ray fluorescence (XRF) analysis across the profundal basin revealed more rapid sediment accumulation in the SW quarter of the lake (see Schillereff et al., 2016b). This pattern and the historical inflow configuration guided site selection. We recovered four deep water cores along an inflow proximal to distal transect (Figure 1D) and short gravity cores (16 – 25-cm length, 8-cm diameter; Boyle, 1995) to capture the sediment-water interface, which were extruded and sliced at 0.5-cm intervals (Table 1). The longer record was sampled as 1- or 1.5-m drives using a hand-percussive Russian-type corer (7.5-cm diameter). A 10-cm overlap was applied to successive drives to ensure a continuous sequence was recovered. Complete sediment profiles varied in length between 1.35 and 3.5 m (Figure 3; Table 1). Drives were retained in plastic guttering, sealed tightly in polythene sleeving and stored at 4°C.

A digital line-scan photograph of the core BW16-3 surface was taken using a Geotek Multi-sensor core logger (MSCL-XZ) (University of Liverpool) prior to sub-sampling and x-radiographic greyscale images of sediment density were acquired on the Itrax core scanner housed at the National Oceanography Centre–Southampton (Croudace et al., 2006). The lack of a visual stratigraphy precluded event sampling thus sediments were subsampled at 5-mm contiguous intervals (Table 1). All samples were weighed, freeze-dried and re-weighed after drying to estimate moisture content. Bulk densities were calculated using the known dry mass of quartz (2.65 g cm^{-3}) given it dominates the catchment bedrock (Chambers, 1978).

3.2 *Sedimentology and geochemistry*

Geochemical composition was determined by XRF analysis (Table 1). Master core BW11-2 was measured as dry sediment on a Bruker S2 Ranger Energy Dispersive (ED)-XRF under a helium atmosphere at three x-ray intensity settings (20, 40 and 50 keV tube excitement). Dry, homogenised loose powders were pressed into sample cups lined with 6 µm polypropylene film. Mass attenuation for each sample was corrected for organic matter content, calculated thermogravimetrically (PerkinElmer S6000) as the mass loss between burn intervals of 230° and 530°C under a nitrogen atmosphere. Cores BW11-3, BW12-9 and BW16-3 were measured non-destructively on a wet sediment basis using either a hand-held Thermo-Niton (2 W Rh X-ray tubes) or an Olympus Delta ED-XRF (4 W) mounted to the Geotek. Cores were measured under Soil mode (40 kV, 40 kV (filtered) and 15 kV beam intensities applied successively for 20 seconds) for heavier elements and MiningPlus mode (40 kV and 15 kV) for lighter elements. Each XRF instrument is subject to regular consistency checks made using a library of certified geochemical reference materials (Boyle et al., 2015). Potential matrix effects induced by variable down-core water content when measuring wet sediments were negated by conversion to a dry-mass basis following the procedures outlined in Boyle et al. (2015), using 5-cm interval training sets. Comparison with BW11-2 dry concentrations verified data ranges.

Table 1. Sampling and measurements details of the four sediment cores.

Core label	Core length (cm)	Measurement resolution (cm)	XRF instrument	Other proxies
BW11-2	350	0.5	S2 Ranger	Particle size
BW11-3	264.5	0.5	Thermo-Niton	Particle size
BW12-9	135	0.5	Olympus Delta (Geotek)	Particle size
BW16-3	287	0.3	Olympus Delta (Geotek)	Line-scan imagery (Geotek)
				X-radiograph (Itrax)

Particle size measurements were performed on a Beckman Coulter™ LS200 laser granulometer (University of Liverpool). The dimensions of individual grain sizes within discrete classes from 0.375 to 2000 µm were computed using a combined Fraunhofer and Mie optical model. Reference materials of known distribution were measured before and after each sample set and the standard error of all repeat measurements is 2.03%. Organic matter (OM) was digested with a 30% H_2O_2 solution for a period of 24 to 96 hours dependant on OM content

and evaporated to a moist paste on a hot plate. Samples were mixed with a deflocculating solution of 1% sodium hexametaphosphate ($(NaPO_3)_6$) and dispersed ultrasonically to minimise the risk of adhesion between individual grains. Final results were the average of three successive runs after replicate distributions were compared manually to verify complete dispersion. Particle size parameters were calculated using the geometric measurement formulae of Folk and Ward (1957), which are sensitive to the presence of coarse tails (Folk, 1966). End-member modelling using the R package 'EMMAgeo' (Dietze and Dietze, 2019) partitioned the particle size data into statistically meaningful groupings using a principal components algorithm. Individual end-members likely reflect differing sediment sources and transport mechanisms. The procedure is described in detail in Dietze et al. (2012).

3.3 *Dating methods*

We used multiple chronological methods to construct age-depth models for Brotherswater. Radiometric dating (^{210}Pb, ^{226}Ra, ^{137}Cs, ^{241}Am) was applied to BW11-2 and BW12-9 cores by direct gamma assay using Ortec HPGe GWL series well-type coaxial low background intrinsic germanium detectors at the Liverpool Environmental Radioactivity Laboratory (Appleby et al., 1986). Sub-samples were measured at non-regular intervals (BW11-2: 1.5- to 4-cm; BW12-9: 1- to 2-cm), guided by sedimentation rate estimated from the Pb mining profiles.

The legacy of acute metal pollution from Hartsop Hall Mine (Figure 1C) offers well-constrained chronological markers. Records show the mine operated periodically between CE 1696 and 1942 (Tyler, 1992) and rates of ore extraction are in good agreement with down-core Pb trends in all cores (Schillereff et al., 2016b). We incorporated the three most reliable industrial markers (see Schillereff et al., 2016b) into the age-depth model to test and refine uncertainties in the radionuclide dating. These markers represent the onset of Pb mining in CE 1696, peak ore extraction between CE 1863 and 1872 when sedimentary Pb concentrations exceeded 10,000 ppm, and the final phase prior to permanent mine closure (CE 1931-1942).

The full BW11-2 sequence was dated using fourteen ^{14}C measurements (Table 2). Sub-sampling depths were guided by the ages of industrial markers present in the sediment geochemistry. Selected samples were sieved at 160 µm in deionised water and hand-picked for identifiable macrofossils. Non-herbaceous (grass/sedge) and leaf fragments and *Alnus sp.* and *Betula sp.* seeds were prioritised but several samples produced a fraction of the required dry organic matter. To overcome this problem, the following sequential procedure was followed until sufficient material was obtained: (i) adjacent depths were sieved; (ii) wood and bark fragments were extracted, recognising the risks of slow decomposition and remobilisation; (iii) all visible plant remains were aggregated. Aggregated samples may have

incorporated aquatic and partially decomposed moss and reed remains, however, so a freshwater radiocarbon reservoir effect related to the release and uptake of 'old' dissolved organic carbon by aquatic plants is a possibility. $\delta^{13}C$ measurements for each submitted radiocarbon sample help elucidate the provenance of submitted material. All fall within the range of terrestrial C3 plants (-25 – -30 ‰; Meyers and Ishiwatari, 1993) with the most negative values potentially indicating the presence of aquatic macrophytes. Given the catchment is underlain by rocks of the Borrowdale Volcanic Series with low $CaCO_3$ content (volcanic-clastic sandstones, lapilli tuffs, andesite and dacite), hardwater issues related to carbonate bedrock are negligible. A critical evaluation of our confidence in each submitted sample (Table 2) guided subsequent age-depth modelling. Radiocarbon measurements were performed at the NERC Radiocarbon Facility (East Kilbride) after a standard pre-treatment using an Acid-Alkali-Acid wash to remove dissolved humic acids, conversion to carbon dioxide by combustion in quartz tubes and graphitisation by iron-zinc reduction. The primary age-depth model was generated for BW11-2 using the Bayesian routine 'Bacon' (Blaauw and Andrés Christen, 2011) in R version 3.5.1 (R Core Team, 2018). The model integrated age information for the sediment surface (CE 2011), artificial (^{137}Cs and ^{241}Am peaks) and natural (^{210}Pb) radionuclide chronologies, ^{14}C ages and Pb mining markers.

3.4 Time series analysis of particle size data

Long-term variations in sediment supply from catchments to lake basins may alter the association between hydrology and particle size through time. We used the time series outlier-detection function in R package 'tsoutliers' (López-de-Lacalle, 2017) in R version 3.5.1 (R Core Team, 2018) to isolate the particle size signal of individual floods in this dynamic sediment regime. This function implements the autoregressive integrated moving average approach of Chen and Liu (1993) to account for non-stationary environmental data. It takes the form ARIMA(*p, d, q*), where *p* is the number of time lags of the autoregressive model, *d* reflects the number of differencing steps to eliminate non-stationarity and *q* represents the order of the moving average model. Outliers are identified where the *t*-statistic (*T)* is greater than two. These T>2 outliers in the particle size record represent anomalously coarse material that we interpret as deposits lain down during high-magnitude floods. Two types of outliers were considered: a temporary change (TC), which represents a marked initial impact with no lasting system memory, and an innovational outlier (IO), which influences some subsequent observations before returning to background sedimentation. We hypothesise that this separates abrupt, high-energy events that probably produce the coarsest laminations from

295 **Table 2.** Radiocarbon dates from Brotherswater core BW11-2. The IntCal13 curve was used for calibration (Reimer et al., 2013) within the
296 Bayesian modelling (Blaauw and Andrés Christen, 2011). The quality assessment was judged by material type, sample volume and $\delta^{13}C$ value.

Publication Code	Sample Identifier	^{14}C Enrichment (% Modern ± 1σ)	Conventional Radiocarbon Age (years BP ± 1σ)	Carbon content (% by wt.)	$\delta^{13}C_{VPDB}$ ‰ ± 0.1	Material dated	Sample integrity	Quality assessment ranking
SUERC-48896	BW11-2 RC1 41-42	95.42 ± 0.53	377 ± 45	46.3	-27.765	Small leaf and wood fragments	High sample volume	GOOD
SUERC-48897	BW11-2 RC2 49-50.5	95.48 ± 0.53	371 ± 45	43.7	-27.879	Leaf, wood and bark fragments, *betula sp.* seeds	Moderate sample volume	MODERATE
SUERC-48898	BW11-2 RC3 61-62.5	97.55 ± 0.54	199 ± 45	48.7	-28.3	Wood fragment, *alnus sp.* seed	High sample volume	GOOD
SUERC-48899	BW11-2 RC4 81-81.5	97.02 ± 0.54	243 ± 45	44.2	-26.098	Small leaf fragment, moss	High sample volume, possible moss misidentification	MODERATE
SUERC-48903	BW11-2 RC6 127-128.5	89.84 ± 0.50	860 ± 45	40.6	-27.351	Wood fragments, *Betula sp.* seed	Very low sample volume so all visible plant remains taken	POOR
SUERC-37679	BW11-3 137.5-138.5		200 ± 30		-28.0	Large leaf fragments, *betula sp.* seed	High sample volume	EXCELLENT
SUERC-48904	BW11-2 RC7 150-151	90.38 ± 0.51	812 ± 45	41.2	-29.119	Leaf and wood fragments, moss, *Betula sp.* seed	Moderate sample volume, possible moss misidentification	MODERATE
SUERC-48906	BW11-2 RC9 172-174	92.26 ± 0.52	647 ± 45	50.5	-28.752	Tiny leaf and wood fragments, assorted unidentified macrofossils	Very low sample volume so all visible plant remains taken	POOR
SUERC-48907	BW11-2 RC10 197-198.5	90.85 ± 0.52	771 ± 46	46.1	-27.862	Tiny leaf and wood fragments, assorted unidentified macrofossils	Very low sample volume so all visible plant remains taken	POOR
SUERC-48908	BW11-2 RC11 224-224.5	92.99 ± 0.54	584 ± 47	54.9	-30.719	Assorted organic macrofossils, *Betula sp.* seed	Moderate sample volume	POOR DUE TO LOW $\delta^{13}C$

SUERC-35378	BW11-2 (3) 258		930 ± 30		-25.0	*Alnus glutinosa* cone	High sample volume, single target	EXCELLENT
SUERC-48909	BW11-2 RC12 269-270	87.03 ± 0.49	1116 ± 45	53.7	-28.506	*Alnus sp.* seed, bark, wood	Moderate sample volume	GOOD
SUERC-48910	BW11-2 RC13 321.5-323.5	84.08 ± 0.47	1393 ± 45	50.4	-28.959	*Betula sp.* seed, large leaf fragment	High sample volume	EXCELLENT
SUERC-48913	BW11-2 RC14 335.5-336	82.66 ± 0.46	1530 ± 45	52.5	-28.384	*Alnus sp.* seed, multiple leaf and wood fragments	High sample volume	EXCELLENT
SUERC-35378	BW11-2 (3) 258		930 ± 30		-25.0	*Alnus glutinosa* cone	High sample volume, single target	EXCELLENT

297

298

floods causing greater fluvial erosion and charging the system with excess coarse material, potentially inducing a new baseline particle size regime.

4. RESULTS

4.1 Chronostratigraphy

Two peaks in ^{137}Cs are relatively well-defined in BW11-2 and BW12-9 (Schillereff et al., 2016b) and a widespread phenomenon in the Brotherswater radioisotope stratigraphy (Semertzidou et al., 2019). The deeper peak coincides with maximum ^{241}Am concentrations, which we attribute to CE 1963 atmospheric nuclear weapons testing fallout. The more recent spike records the CE 1986 Chernobyl fallout. These markers corroborate the ^{210}Pb-derived chronology, which for BW12-9 extends to CE 1880 (Schillereff et al., 2016b). Unsupported ^{210}Pb concentrations decline exponentially with depth, enabling sedimentation rates to be calculated using the Constant Rate of Supply (CRS) model (Appleby et al., 1978).

The 'Bacon' model (Figure 2) implemented Markov Chain Monte Carlo repetitions constrained by a gamma distribution with mean 5-yr mm^{-1} and shape 2 and a beta distribution with mean 0.5 and memory strength 20. The ^{14}C ages were calibrated using the IntCal13 curve (Reimer et al. 2013). The mining markers were integrated into the 'Bacon' framework using narrower Student's-*t* uncertainty distributions (i.e., parameters *t.a* and *t.b* were set to 33 and 34, respectively) that reflect their greater chronological certainty.

The primary 'Bacon' age-depth model, in which all ^{14}C distributions were treated as equally likely, reveals stratigraphic coherence in the lower core but a number of possible outlier radiocarbon ages at shallower depths (Figure 2A). The deepest four ^{14}C ages are judged to be reliable on the basis of stratigraphic alignment and high volumes of identifiable terrestrial leaves and seeds (Table 2). They also predate problems with 'old carbon' previously identified during ^{14}C dating of bulk sediments deposited after 1000 cal. BP (Chambers, 1978), a window which overlaps with the more problematic ^{14}C measurements in our record. In the current age depth model, the pair of uppermost ages (41- and 50-cm depth) have good sample integrity (Table 2) but plot as 'too old', given the secure ^{210}Pb curve and CE 1930s mining marker. Kirkstone Beck underwent a pronounced channel straightening between CE 1860 and 1890 (see Section 2.2) and the new channel cuts through the fringing wooded peatland on the southern shore. This may have supplied 'old' macrofossils, affording an explanation for these anomalous ages. Three ^{14}C ages (61-cm, 81-cm and 135-cm depth) return broad probability distributions with multiple equally-likely age solutions (Figure 2A). This pattern reflects the tiered plateaus in the CE 1700-present ^{14}C dendrocalibration curve induced by fossil fuel combustion (Hua, 2009). The CE 1860s and CE 1696 industrial pollution markers are helpfully positioned to anchor each of these ages, however. The middle portion (125-225 cm) of the

core is more problematic because six ^{14}C ages do not follow a coherent stratigraphical order. We rule out hardwater effects given Brotherswater lies in a non-carbonate catchment and the Ca profile mirrors elements (K, Ti) sourced from the volcanic bedrock. The deepest Pb marker secures the ^{14}C age at 134 cm, an interpretation that suggests the ^{14}C ages at 128- and 151-cm depth are 'too old'. Lakes across the region have shown age reversals during the late-Holocene, including at Brotherswater (Chambers, 1978), that were attributed to mobilisation of 'old carbon' locked in soils and delivered to the lakes during landscape clearance episodes (Pennington, 1991; Edwards and Whittington, 2001; Chiverrell, 2006). While this is a greater concern when dating bulk material, which we have avoided, the risks are not eliminated. The most problematic samples yielded low volumes of suitable material. In these cases, all visible plant remains were aggregated, including woody and unidentifiable organic fragments, meaning sample integrity was poor (Table 2). Wood can experience slower decomposition rates and be washed into a lake decades or centuries later (Barnekow et al., 1998). Given the small sample weights, wood fragments would contribute towards older than expected ages. The unidentified materials could also have included aquatic plants and reeds from the fringing wetland. While the $\delta^{13}C$ measurements indicate a terrestrial provenance for most dated material (Meyers and Ishiwatari, 1993), these problematic samples are more depleted in ^{13}C, which could mean submerged aquatic macrophytes have been sampled (Osmond and Roksandic, 1981). There is also geomorphological evidence for larger-scale remobilisation of catchment materials during this time window. An incised debris cone in the Brotherswater catchment ^{14}C-dated to CE 1000-1200 (Clark et al., 2007) illustrates how gully reactivation could erode and release less-decomposed plant macrofossils from a buried organic hillslope deposit. This gully inception event has parallels in the wider region, with Chiverrell et al. (2007; 2008) constraining major expansions of hillslope erosion and gully networks across northwest England to this period.

Two parsimonious scenarios for the age-depth model are presented in Figures 2A and 2B. The first uses older ages at 173 and 198-cm depth based on our evaluation of sample integrity to minimise sampling of aquatic material (very negative $\delta^{13}C$) and the impacts of reworked old carbon. The second scenario (Figure 2B) treats those ^{14}C measurements as maximum age estimates, given the potential for reworking, and assumes, *a priori*, that the youngest age at 224-cm is reliable. Implications of each age-depth model are explored in later discussion.

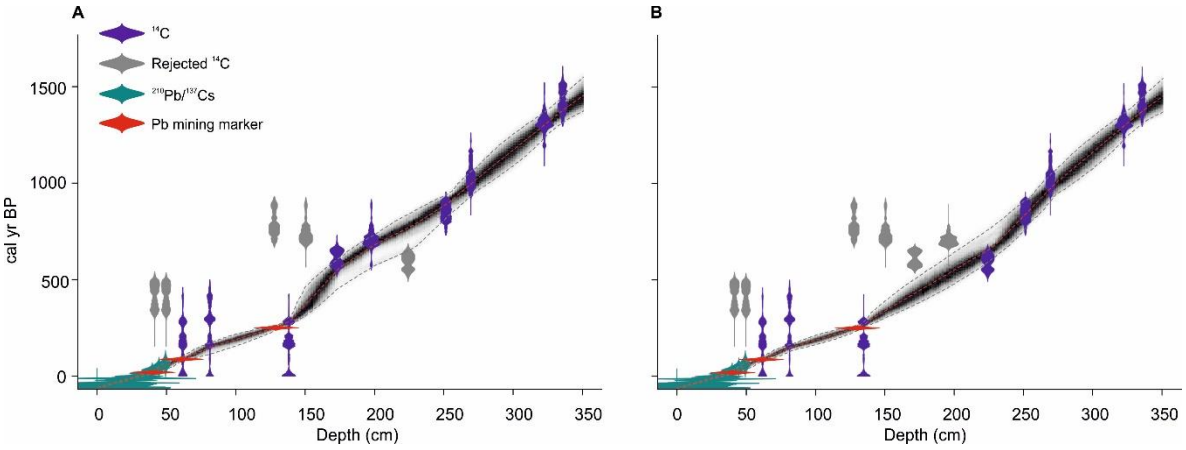

Figure 2. A) 'Bacon' age-depth model for core BW11-2 based on fourteen radiocarbon ages, ^{210}Pb and ^{137}Cs radionuclide dating and three reliable Pb mining markers: the onset of mining in CE 1696, peak ore extraction (CE 1863) and the final phase prior to mine closure (CE 1931). **B)** Scenario B assumes, *a priori*, a reliable date at 224-cm below four sequential ^{14}C reversals. See text for further discussion.

Modelled ages are quoted as weighted means in the output from 'Bacon'. The primary chronology extends to CE 519, although depths 335–351 cm follow a linear extrapolation from the deepest ^{14}C age. This 1500-year sediment sequence represents, to date, the longest lake-derived palaeoflood record in the UK. Maximum and minimum 95% confidence age ranges are 2.9 (2-cm depth) and 190 (225-cm depth) years, respectively. Sedimentation rates at core site BW11-2 are fairly high throughout the record (mean 0.26 cm yr^{-1}), with most rapid accumulation since the CE 1870s. The BW11-2 chronology was transferred to other cores based on the repeatable geochemical stratigraphy for multiple elements across the basin (Schillereff et al. 2016b).

4.2 Sedimentology and geochemistry

The dominant constituent of all cores is a visually homogeneous, grey-brown limnic mud, which our monthly sediment trapping showed is regular background sedimentation (Schillereff et al., 2016a). Some variation in sediment colour occurs at the decimetre scale, with lighter deposition paralleling increased bulk density (0.3–0.8 g cm^{-3}), reduced organic matter content (5-8% lower) and higher concentrations of elements reflecting catchment mineral supply (Ti, Zr) (Figure 3). The upper sediments in all cores shift to very dark brown to black (above 60-cm in BW16-3). Occasional light-brown layers are visible as higher density features in ITRAX radiograph images (e.g., 90- and 100-cm depth in BW16-3; Figure 3). This stratigraphy suggests cores are not affected by bioturbation, reinforced by tight repeatability across the XRF geochemistry and particle size profiles. A systematic visual signature of coarser material

396 does not emerge from the background matrix, however, so detection of flood layers depends
397 on high-resolution particle size measurements.
398
399

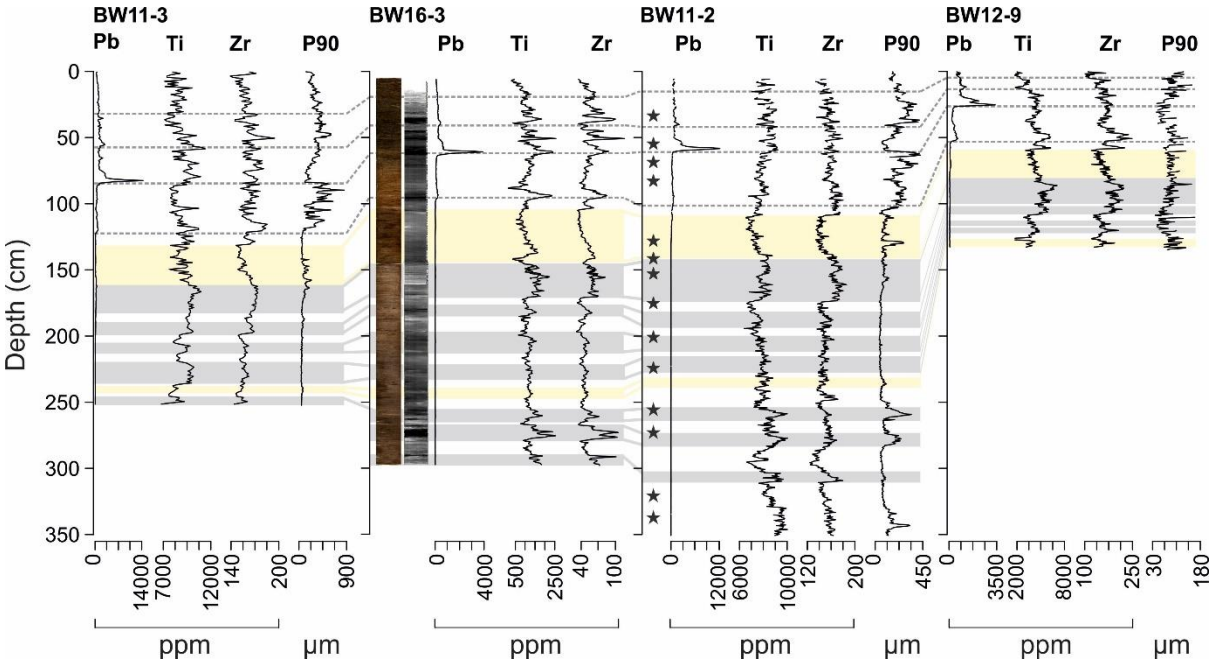

400
401

402 **Figure 3.** Lithology of Brotherswater cores, plotted from left to right as moving from the inflow
403 (BW11-3) to the basin centre (BW12-9). The Pb profile mirrors the catchment mining history,
404 Ti and Zr are interpreted as proxies for minerogenic input from eroded soils and bank erosion
405 and the 90th percentile (P90) of particle size distributions isolates the coarsest fraction. Dashed
406 grey horizontal lines denote prominent shifts in Pb profiles in all cores, grey boxes show
407 matching Ti and Zr horizons and beige boxes are based on links between particle size profiles.
408 Stars represent sampling depths for radiocarbon dating in BW11-2.
409

410 *4.3 Particle size*

411 Variation in the calibre of deposition in Brotherswater is observed across all cores (Figure 3)
412 at multiple scales. The dominant mode in most particle size distributions (PSDs) lies in the silt
413 range and reflects background sedimentation. The coarsest deposition lies in the sand
414 domain, with maximum P90 ($P90_{max}$) in BW11-3 exceeding 800 µm. We calculate the 90th
415 percentile (P90) for the particle size distributions to focus on size variations in the coarsest
416 fraction, which requires the greatest fluvial energy to transport. Zones of decimetre thickness
417 characterised by coarser deposition are a feature of all cores (Figure 3) and this longer-term
418 variation is overprinted by thin (5-20 mm), sharp peaks that reflect more abrupt depositional
419 events. Most intervals of coarse deposition coincide with phases of elevated mineral supply

(Ti and Zr; Figure 3). This association breaks down on occasion, though, most notably when finer sediments were deposited after peak mining while Ti and Zr concentrations remain high.

End-member modelling analysis (EMMA) confirms these patterns of particle size deposition. Sensitivity tests following Dietze et al. (2012) using a low weight transformation (0.005; R^2 = 0.86) reveal the optimum number of end-members capable of explaining more than 95% of the variance in the dataset is 3 (4 in BW12-9). The EMMA decomposes the particle size distributions into three end-member groupings with modes in the clay, medium silt and fine/medium sand (Figure 4). Four end-members were required to model BW12-9 (explaining 86% of the variance) including an additional coarse-silt component (EM3) and a significantly finer sand class (EM4 mode = 146.82 µm) in this more distal sector of the lake.

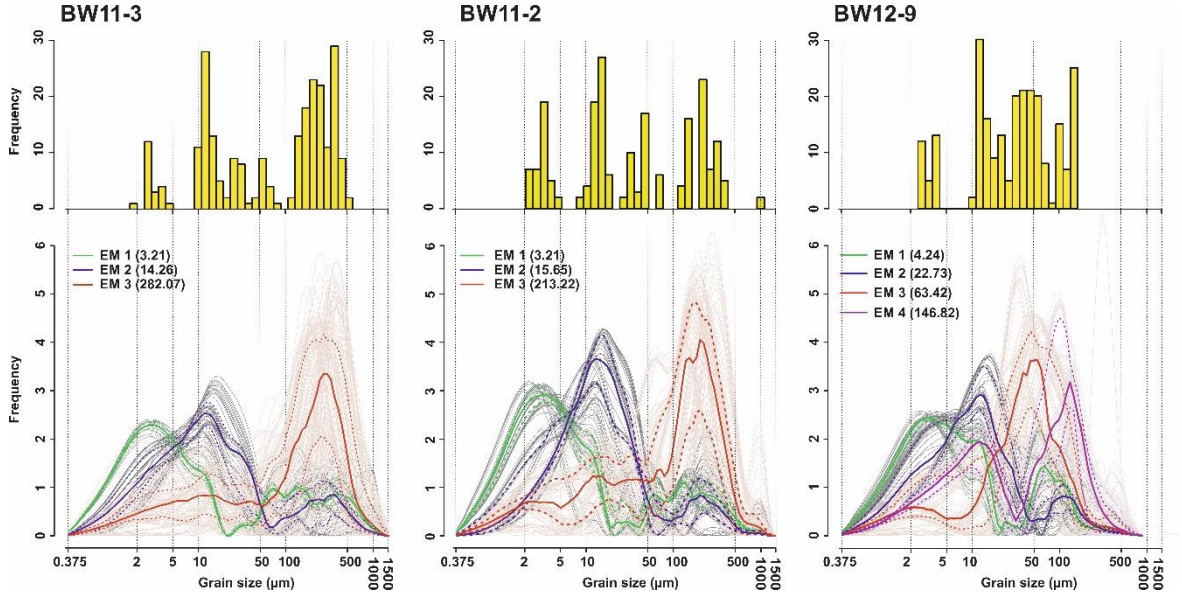

Figure 4. Modal histograms and unmixed particle size distributions from the optimal end-member models. Solid (dotted) lines represent mean (±2σ) of the robust end-members. Green: clay/very fine silt EM1; blue: fine/medium silt EM2; red: fine sand EM3. Note BW12-9 deciphers four end-members: red: coarse silt (EM3); purple: very fine sand (EM4).

Most PSDs in all cores are uni- or bi-modal so the use of conventional frequency statistics is appropriate (Beierle et al., 2002). Laser diffraction instruments most effectively differentiate silt-dominated samples (Roberson and Weltje, 2014), further increasing our confidence in the robustness of the particle size measurements. Lastly, plotting mean versus sorting and skewness and skewness versus sorting produces sinusoidal, circular and helical curves, respectively, patterns commonly observed in other depositional settings (Folk, 1966).

446 *4.4 Particle size-inferred flood series*

447 Variation at the decimetre scale in Ti and Zr mirrors the P90 profiles and points towards a non-
448 stationary sediment regime through the late-Holocene (Figure 3). The *tsoutliers* package fitted
449 an ARIMA(2, 1, 1) model and, based on the recommended sensitivity threshold (*T*) of 2,
450 isolated 88 anomalously coarse deposits through the 1500-year record (Figure 5B). Discrete
451 deposits in BW11-2 and BW11-3 show a strong stratigraphical match since CE 1800, the
452 period for which independent hydrological data are available (Figure 5A). A total of 31 flood
453 units can be correlated in stratigraphic sequence within the chronological uncertainty of the
454 age models. The unit at the top of BW11-3 almost certainly corresponds to the major 2009
455 regional flood. Two *T*>2 units (weighted mean year of deposition: 1998 and 1854) detected in
456 BW11-2 cannot be linked to an equivalent deposit in BW11-3, although in both cases an outlier
457 slightly below the T>2 threshold occurs. The 1862 flood is also difficult to correlate but could
458 be part of the unit 22 cluster. Further back in time, equivalent matches are most notable during
459 the flood-rich 18th and 15-16th centuries (Figure 5B). The set of outlier deposits dated between
460 CE 1620 and 1660 in BW11-2 are problematic as they are absent in BW11-3. This raises
461 some concerns about record fidelity but, overall, the CE 1800-present and long-term matches
462 are promising.

463 Overall, particle size outliers representing discrete floods are not equally spread
464 through time. Rather, based on the primary age-depth model for BW11-2, clusters of coarse
465 deposits occur at CE 510-630, 890-960, 990-1080, 1470-1560, 1590-1620, 1650-1710, 1740-
466 1770, 1830-1890 and since 1920. Using a time window of equivalent duration to regional
467 gauged river flow series and the standard climate regime (i.e., 30 years), event frequency
468 during flood-rich episodes is 2-8, falling to one or zero events during intervening periods
469 (Figure 7C). Intervals of low or inactivity are longer (>200 years) in the earlier record.

470

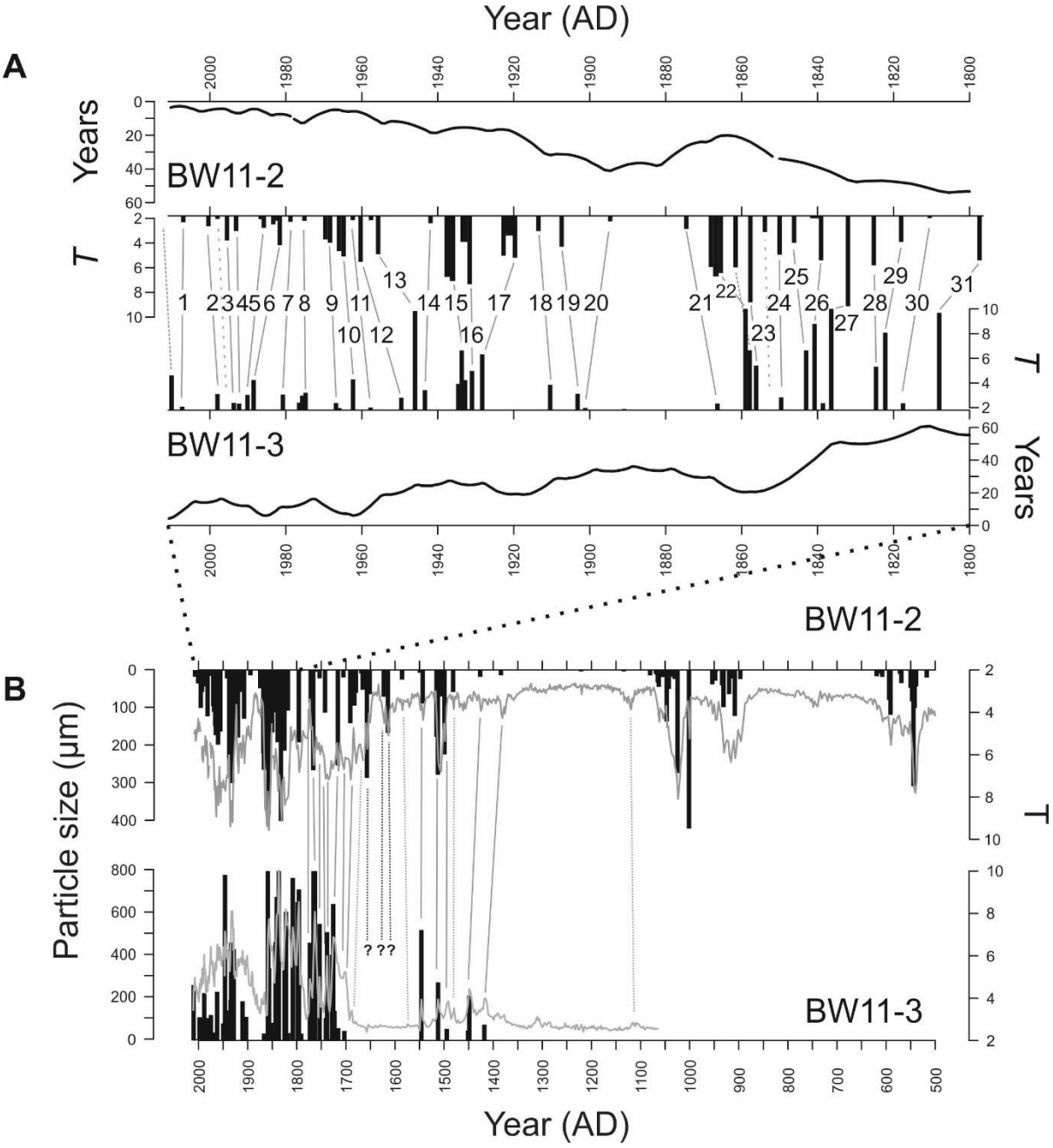

Figure 5. A) An event-scale comparison between the *tsoutliers*-derived palaeoflood record for BW11-2 and BW11-3 spanning CE 1800-2010. This interval is explored in detail because contemporaneous independent instrumental and historical flood records are available (see Figure 6; Section 5.1). Grey lines show matched flood units that follow stratigraphic sequence and fall within the chronological uncertainty of both cores. The CE 2009 deposit was not recovered at the surface of BW11-2. Long dashed lines indicate minor above-threshold deposits in BW11-2 that cannot be correlated to a BW11-3 layer. Sequential above-threshold deposits are considered single events. The solid line plots depict the minimum to maximum age difference for BW11-2 and BW11-3. B) Stratigraphic correlation of the *tsoutliers*-derived palaeoflood record for BW11-2 and BW11-3 spanning the last ~1000 years. We infer outliers

where values with $T>2$ were detected in the ARIMA model applied to the 90th percentile (P90) profiles. Solid vertical lines denote matched flood deposits and dashed lines cannot be linked to a corresponding flood unit in BW11-3.

5 Discussion

5.1 The Brotherswater palaeoflood record

Our study has produced the longest lake-based palaeoflood record for the UK, with 88 flood units identified since CE 500 (core BW11-2). The record is characterised by periods of high-frequency flooding at CE 510-630, 890-960, 990-1080, 1470-1560, 1590-1620, 1650-1710, 1740-1770, 1830-1890 and since 1920 (Figure 5B; Figure 7C). Few flood records of comparable length exist in the UK, although Jones et al. (2012) also showed frequent flooding CE 800-1200 followed by a multi-centennial absence and a recurrence after CE 1550 along the River Severn. This broader tendency for floods to cluster at the multi-decadal scale is evident in palaeoflood reconstructions from the UK (Foulds and Macklin, 2016; Macdonald and Sangster, 2017), western and central Europe (Arnaud et al., 2016; Benito et al., 2008; Wirth et al., 2013b) and further afield (Munoz et al., 2018). This behaviour has implications for flood frequency analysis: trends identified in a 30-year flow record may be artefacts if that time window is unrepresentative of the longer-term hydrological regime (Hannaford, 2015; Hooke, 2006).

Over the historical era (post-CE 1800), the timing of most flood-rich episodes (especially the late-19th century) aligns with regional historical flood records (Macdonald and Sangster, 2017; Parkes and Demeritt, 2016; Pattison and Lane, 2012) but diverges elsewhere (e.g., before CE 1850). Archive sensitivity is likely to be a crucial factor. Pattison and Lane (2012) compiled documentary evidence of 137 floods in Carlisle since CE 1770 (see Figure 1B for location), whereas we identified only 32 flood deposits since CE 1800. Historical records from Carlisle such as newspaper accounts probably document most overbank inundations, whereas sediment trapping in Brotherswater showed that a discharge threshold controls flood unit preservation (Schillereff et al., 2016a). Encouragingly, our lake reconstruction shows good agreement to the highest-magnitude floods since CE 1800 at Carlisle estimated from documentary sources (Parkes and Demeritt, 2016; Smith and Tobin, 1979). Rather than directly integrating these dates into the Brotherswater chronology, a systematic comparison shows our age probability distributions for 14 of 16 flood units overlap with the highest-ranked river discharges between CE 1800 and 1930 (Figure 6). Instrumental data spanning the 20th century produce a comparable match. Moreover, 96% of these events occurred between October and March, confirming our reconstruction primarily represents a winter flood reconstruction.

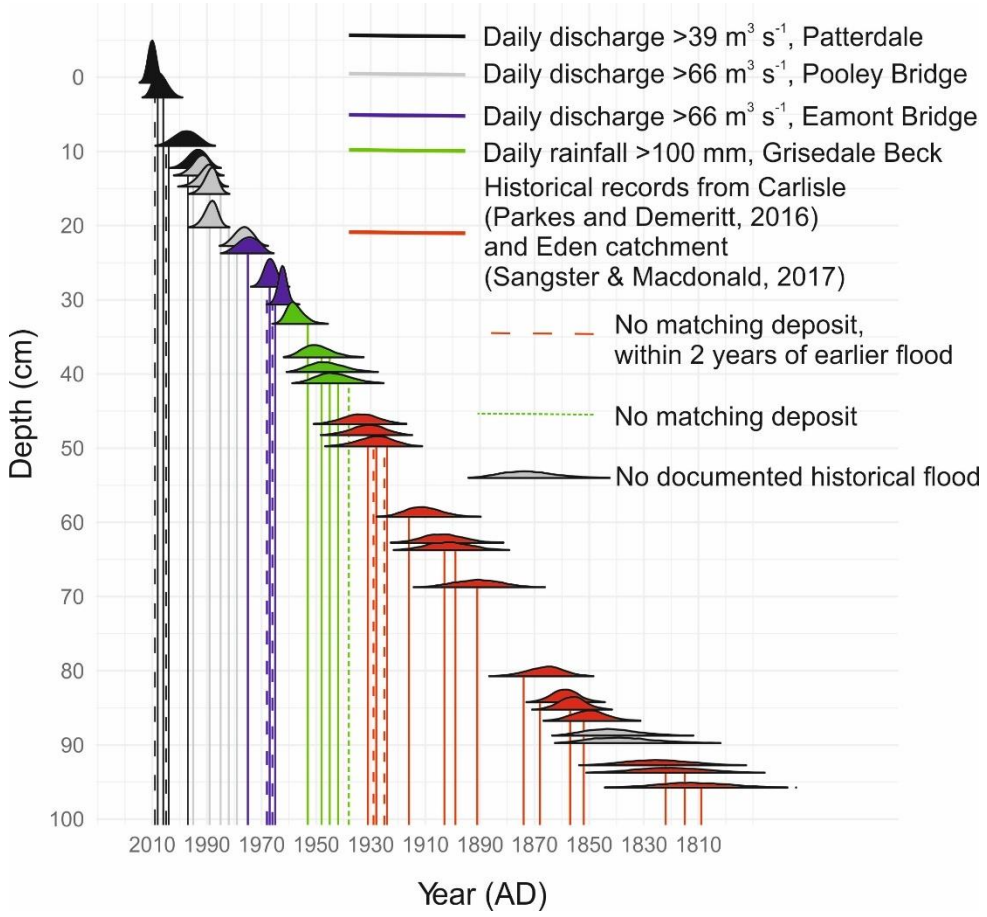

Figure 6. Age probability distributions of flood deposits identified in the BW11-3 ARIMA model generated using the R package 'ggjoy' (Wilke, 2018) and the Bacon.Age.d() function. Vertical lines denote independently-recorded hydrological extremes: black line = above-threshold discharges at Patterdale Side Farm; grey lines = Pooley Bridge; blue lines = Eamont Bridge discharge; green lines = daily rainfall >100 mm at Grisedale Beck; red lines represent years with major historically documented floods at Carlisle (Macdonald and Sangster, 2017; Parkes & Demeritt, 2016). See Figure 1B for monitoring station locations. Discharge thresholds for flood deposit preservation were established from sediment trap monitoring described in Schillereff et al. (2016a). Dashed lines reflect documented floods without a matching deposit but where a flood occurred within the preceding 1-2 years. The green, short dashed line cannot be stratigraphically ascribed to a deposit.

There are some stratigraphical mismatches. A succession of five documented floods in the 1920-30s corresponds to three flood deposits. We propose event sequencing as the most plausible explanation for events being under-represented in the sedimentary record (Magilligan et al., 1998). There is widespread evidence that catchment sediment stores are flushed during major floods, leaving insufficient material to fully exploit the transport capacity

of subsequent high flows (Cockburn and Lamoureux, 2008; Kämpf et al., 2014). Pulses in sediment availability can be a key factor in determining the scale of sedimentological and geomorphological change during major floods (Hooke, 2015). At Brotherswater, Chambers (1978) noted the suspended sediment load plummeted nearly 100% through three successive floods of equivalent rainfall and discharge. Our contiguous 0.5-cm sampling strategy should not miss the sedimentary signal of annual maximum flows because sedimentation rates through that section (0.55 cm yr^{-1}) approximates to annual resolution and documented floods occurred 1-2 years apart. Using the contemporary discharge thresholds established for Brotherswater (Schillereff et al., 2016a) means twelve of sixteen 20th-century floods can be tied to a discrete deposit (Figure 6). Removing sub-two-year flood couplets produces a like-for-like match to the independent hydrological records presented in Figure 6, suggesting the timescale for sediment recharge is approximately two years. These supply-limited characteristics generate a non-linear discharge-sedimentation pattern, meaning signatures of high flows may on occasion not be preserved (Magilligan et al., 1998; Sambrook Smith et al., 2010). As a result, Brotherswater provides a record of sedimentologically and geomorphologically significant floods. While this precludes attempts to estimate historical event magnitudes, our reconstruction provides a conservative estimate of flood frequency and reliably identifies the timing of multi-decadal flood-rich and flood-poor episodes.

Table 3. The ten highest daily maximum discharges at three gauging stations progressively downstream from Brotherswater (see Figure 1B for locations) for the period 02/02/1997 to 01/01/2011 (the operational lifespan of Patterdale Side Farm station). Green shades indicate a Top 10 flood at all sites and brown shades denote Top 10 at Pooley Bridge and River Lowther. For clarity, lighter colours represent progressively more recent events.

Daily Maximum Rank	Patterdale Side Farm	Pooley Bridge	Eamont Bridge
1	November 2009	November 2009	November 2009
2	January 2005	January 2005	January 2005
3	February 2004	December 2006	February 2002
4	October 2008	February 1997	February 2004
5	December 2006	February 2004	October 1998
6	February 1997	October 2008	December 2000
7	September 2004	December 2000	December 2006
8	December 1999	October 1998	February 1997
9	December 2007	February 2002	January 1999
10	July 2009	January 2009	October 2008

Two deposits in the 1840s do not correspond stratigraphically to known floods. The region is susceptible to spatially heterogeneous, orographical rainfall (Burt and Howden, 2013), meaning localised, intense convective precipitation events can occur that may not trigger flooding in Carlisle ~43 km downstream (Figure 1B). That said, the highest-magnitude floods appear to persist across the Eden catchment (Table 3). Overall, our evidence suggests an encouraging degree of fidelity to the Brotherswater palaeoflood record.

5.2 Depositional mechanisms under high-flow conditions

Pb profiles that shallow towards the lake centre confirm that fluvial supply dominates lake sedimentation (Figure 3; Schillereff et al., 2016b). This is mirrored by fining grain sizes towards the basin centre, where sediments are also, on average, better sorted and less negatively skewed. This processing by the lake reflects decelerating fluvial plumes. The negative correlation between particle size and skewness (r = -0.60) shows the suspension of excess fine particles under high flow conditions that eventually fill the pore spaces in coarse deposits (Bøe et al., 2006). We interpret these patterns to indicate inflow dynamics are dominated by homopycnal or mesopycnal, laminar flows (Cockburn and Lamoureux, 2008; Kämpf et al., 2014). Brotherswater displays no thermal stratification during winter when most floods occur and flood waters are warmer than the ambient lake temperature (Schillereff et al., 2016a). As a result, the less dense plume expands laterally near the lake surface and particles settle vertically at rates dictated by their diameter and mass. This explains why the central and delta-distal sectors are less sensitive to floods and preserve fewer coarse deposits (Figure 3; Schillereff et al., 2016a). This depositional mechanism contrasts with lakes that experience powerful turbidity currents capable of transporting coarse material extended distances across the lake bed (Girardclos et al., 2007; Osleger et al., 2009; Sturm and Matter, 1978). Basin slope angle is susceptible to seismic destabilisation (Wilhelm et al., 2016) but we do not observe sedimentological features associated with 20th-century regional seismicity (Fielding et al., 2018) nor can any abnormal deposit be linked to the largest documented historical earthquake (CE 1247, Irish Sea, Mw = 5.47 ± 0.47; Stucchi et al., 2013).

These basin-wide sediment dynamics indicate particle size measurements can reliably detect high flows, overcoming challenges posed by the dark brown, homogeneous sediment matrix. This was reinforced by sediment trapping over an 18-month period (Schillereff et al., 2016a), which detected a particle size and discharge thresholds for flood deposits. Earlier sediment-source monitoring at Brotherswater (Chambers, 1978) captured particle size distributions that mirror our end-member populations (Figure 4) and showed high flows dominate the transport of coarse material. The fine-grain EM1 (mode = 2-5 μm) most likely

599 represents suspended sediment derived from weathering and erosion of catchment soils. Its
600 similar proportion across the basin can be explained by prolonged suspension. The medium-
601 silt EM2 (10-40 µm) is the dominant component under regular flow conditions, especially to
602 the delta proximal sector of Brotherswater (BW11-2 comprises 50-75% silt). Catchment
603 sampling showed streambank material mostly lies in this fraction (Chambers, 1978), and it
604 also dominated our more recent sediment trapping (Schillereff et al., 2016a). Scour at the river
605 bed and lateral erosion of hummocky moraines on the valley floor are important sources of
606 coarse EM3 material (100-500 µm). Mineralogical evidence shows this calibre can only reach
607 the lake during floods (Chambers, 1978) and sediment trapping during the most recent major
608 flood in the region (Storm Desmond, winter 2015; Chiverrell et al., 2019) produced P90 values
609 coarser than 500 µm.
610
611 ***5.3 Climate drivers of flooding in northwest England***
612 Comparing the frequency of flooding at Brotherswater with a proxy winter NAO record (Proctor
613 et al., 2002) shows a significant, negative correlation (r = -0.65, $p<0.001$; Figure 7E). The CE
614 890-960 and 990-1080 flood-rich periods align with minor NAO negative excursions and
615 sedimentary evidence for floods is scarce through the persistent positive NAO phase CE 1100-
616 1400 (Baker et al., 2015; Trouet et al., 2009). Subsequent flood-rich episodes follow negative
617 NAO behaviour. The alternative chronology also returns a significant correlation. The
618 Brotherswater record shows good agreement to a reconstruction of autumn and winter
619 flooding from central Spain (Figure 7D; Benito et al., 2003), a region subjected to the same
620 moist westerly air-masses from the North Atlantic. This reinforces historical and instrumental
621 evidence that negative winter NAO conditions are an important driver of UK and pan-European
622 flood frequency (Foulds and Macklin, 2016; Macdonald and Sangster, 2017; Moreno et al.,
623 2008; Wilhelm et al., 2012; Wirth et al., 2013a) as the mid-latitude pressure gradient exerts a
624 strong influence on the genesis of westerly air masses (Jones et al., 1997; Wilby et al., 1997).
625 Comparison to the daily weather classification scheme of Neal et al. (2016) confirms westerly
626 systems are a dominant driver of winter flooding. Cyclonic westerly, cyclonic south-westerly
627 or cyclonic west-north-westerly weather patterns occurred in the three days preceding 52%,
628 35% and 39% of floods since CE 1800 (Neal et al., 2016).
629 The Brotherwater record shows four flood-rich episodes overlap with solar minima in
630 the 10-11th (Oort), 15-16th (Spörer) and 17-18th (Maunder) centuries (Figure 7D). This fits well
631 with proposed mechanisms that link solar lows to persistent atmospheric blocking and
632 southward shift in storm tracks across the North Atlantic, leading to flooding across western
633 and central Europe (Czymzik et al., 2016; Wirth et al., 2013b). The alternative chronology
634 (Figure 2B) places the 15-17th century flood-rich episode slightly more recently but it remains

635 aligned with a solar low. However, other periods of frequent flood activity do not align with
636 solar minima (e.g., CE 520-620, CE 1850-1900 and since the CE 1930s) and flooding was
637 rare during the Wolf solar minimum (13-14th century). The non-significant correlation ($p>0.05$)
638 between Total Solar Irradiance (TSI) and binned flood frequency mirrors the intermittent
639 relationship between solar forcing and UK hydroclimate observed in peat and historical
640 archives (Charman et al., 2006; Macdonald and Sangster, 2017) and suggests that the
641 relationship between solar activity and flood occurrence is complex and probably time-
642 trangressive.

643 The three lengthiest (>50 year) flood-rich episodes since CE 1600 align with positive
644 AMO excursions (Gray, 2004), mirroring patterns in documented floods across western Britain
645 (Macdonald and Sangster, 2017). Overall, there is no significant correlation with the frequency
646 of floods at Brotherswater ($r=0.33$, $p>0.05$) but this is hampered by the short AMO
647 reconstruction. Climate models associate the positive phase of the AMO with increased
648 cyclonic weather systems and greater rainfall over northwest Europe, especially in winter,
649 potentially triggered by enhanced ocean-atmosphere energy transfer from warmer SSTs
650 (Knight et al., 2006).

651 The sediment record indicates floods have been more frequent in the 20th century and
652 in particular since the CE 1930s (Figure 7C). This ties into the persistent negative NAO and
653 positive AMO modes and some independent evidence corroborates this trend, with Macdonald
654 and Sangster (2017) showing frequent high-magnitude floods after CE 1930 in northern
655 England.

656

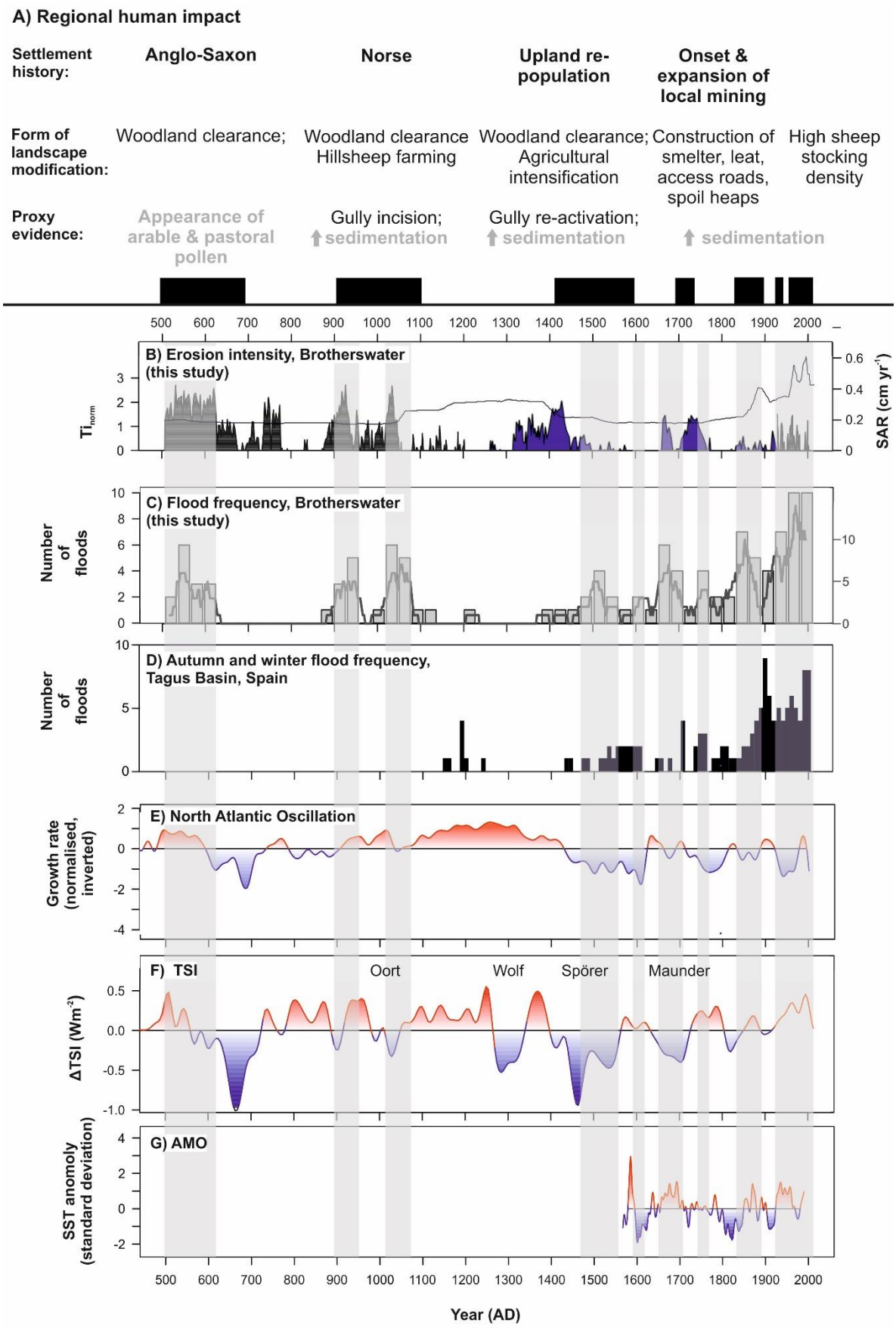
A) Regional human impact
Settlement history:
Anglo-Saxon
Norse
Upland re-population
Onset & expansion of local mining
Form of landscape modification:
Woodland clearance;
Woodland clearance Hillsheep farming
Woodland clearance; Agricultural intensification
Construction of smelter, leat, access roads, spoil heaps
High sheep stocking density
Proxy evidence:
Appearance of arable & pastoral pollen
Gully incision; sedimentation
Gully re-activation; sedimentation
sedimentation
500 600 700 800 900 1000 1100 1200 1300 1400 1500 1600 1700 1800 1900 2000
B) Erosion intensity, Brotherswater (this study)
Ti_norm
SAR (cm yr-1)
C) Flood frequency, Brotherswater (this study)
Number of floods
D) Autumn and winter flood frequency, Tagus Basin, Spain
Number of floods
E) North Atlantic Oscillation
Growth rate (normalised, inverted)
F) TSI
Oort
Wolf
Spörer
Maunder
ΔTSI (Wm-2)
G) AMO
SST anomoly (standard deviation)
Year (AD)

657

Figure 7. A) Summary of regional geomorphological (black text) and palaeolimnological (grey text) evidence for anthropogenic modification of the landscape. References provided in the text. **B)** Normalised Ti from cores BW11-2 (black) and BW12-9 (blue) as a proxy of catchment erosion at Brotherswater. Solid line is BW11-2 sedimentation rate (SR). **C)** Time series of flood frequency at Brotherswater for core BW11-2. Particle size outliers (T>2) were summed into climatically-representative 30-year bins. The dark grey line is the 31-year running sum. **D)** Autumn and winter flood frequency in the Tagus Basin, central Spain, as summed into 10-year bins (Benito et al., 2003). **E)** Normalised growth rate of speleothems from Scotland as a proxy for North Atlantic Oscillation behaviour (Proctor et al., 2002). **F)** Variation in Total Solar Irradiance (TSI) through the late-Holocene (Steinhilber et al., 2009). Known solar minima are labelled. **G)** Reconstruction of the Atlantic Multi-decadal Oscillation, reflected by variations in sea surface temperatures (SST) (Gray, 2004). Vertical grey bars demarcate flood-rich (n > 2) episodes at Brotherswater.

5.4 Human influence on late-Holocene flooding

Six flood-rich episodes (CE 510-630, 890-960, 990-1080, 1470-1560, 1650-1710 and 1830-1890) also overlap with periods of regional agricultural intensification and mining expansion in the catchment (Figure 7A). Woodland clearance and grazing pressure can lower geomorphic thresholds for erosion (Giguet-Covex et al., 2012; Orr and Carling, 2006); the relatively steep slopes and shallow soils around Brotherswater are particularly vulnerable. While the outlier treatment isolates coarse laminations, it does not account for longer-term changes in the catchment sediment conveyor driven by human activity. Ti should be an effective proxy for catchment erosion as it is tightly correlated with K and Zr (Schillereff et al. 2016b), with positive excursions in normalised Ti (Ti_{norm}) profiles distinguishing active soil erosion. The late-Holocene record of minerogenic input to the lake centre (BW12-9) is more sensitive to long-term variations in sediment supply than event deposition (Schillereff et al. 2016a), with BW11-2 used only for the earlier record (Figure 7B).

The earliest three flood-rich episodes align with maximum Ti_{norm} values and regional palynological and geomorphological evidence for greater human impact on the landscape (Figure 7A-B). Flooding in the earliest part of the record (CE 510-630) overlaps with pollen evidence of Anglo-Saxon pastoral activity in the Eden valley (Langdon et al. 2004) while the two periods of frequent flooding between CE 900 and 1100 coincided with major Norse settlement in the region (Winchester, 1987). The resulting expansion of upland sheep grazing triggered slope destabilisation across the region (Chiverrell, 2006; Chiverrell et al., 2007; Pennington, 1991; Wild et al., 2001) and rapid debris cone aggradation in the Brotherswater

catchment was dated to ~CE 1000-1200 (Clark et al., 2007). This mirrors two prominent peaks in Ti_{norm} (Figure 7B). Contemporaneous shifts in climatic drivers are modest, however, considering the amplitude of the flood frequency curve (Figure 7C). An anthropogenically enhanced sediment conveyor and more rapid runoff due to cleared hillslopes that amplified catchment sensitivity to moderate storm activity is the likely explanation.

Expansion of sheep rearing triggered gully re-activation across northwest England (Chiverrell et al., 2007) and faster sediment accumulation in Cumbrian lakes during the 15-16th centuries (Chiverrell, 2006; Pennington and Lishman, 1984). Elevated Ti_{norm} (Figure 7B) provides strong evidence of intense soil erosion around Brotherswater, although this timing precedes the CE 1470-1560 flood-rich episode. The most plausible interpretation involves anthropogenic and climatic interplay. Despite the enhanced erosion regime, only a minor increase in flooding begins around CE 1380 after a three-century lull. We propose that the positive NAO and TSI alone did not create a hydroclimatic regime that favoured flood generation. The later shift to negative wNAO and low solar activity thus swept through a sediment system primed by human modification.

Mining in the Brotherswater catchment started in CE 1696 (Tyler, 1992) and brought an acceleration in sedimentation rate, greater mineral supply and coarser material to the lake (Figure 3; Schillereff et al., 2016b). This pronounced land-use change also kick-starts a steady rise in flood frequency (Figure 7C). This trajectory is most likely a function of anthropogenic perturbations to baseline sediment supply, overprinted by short-lived episodes of climatically induced frequent flooding. Phases of elevated Ti_{norm} align with documented excavation of new mining levels, the diversion of hillslope drainage through a leet (a sluice feeding water towards the mine), smelter construction, dumping of spoil and installation of an access road at Hartsop Hall Mine, in particular during the 19th century (Tyler, 1992). Maximum ore extraction rates in the 1860s (Schillereff et al., 2016b) also delivered darker sediments (Figure 3) while documented fish die-offs were attributed to contaminated mining effluent (Chambers, 1978). A complex system response is evident, however, because fine-grained, minerogenic sediment accumulated more rapidly after peak mining (Figure 3) and the flood signal was notably dampened during the late-19th century (Figure 5B). Channel straightening and levee embankment installation occurred at this time (Figure 1D; Section 2.2), which appears to have mobilised fine bank material (EM2) but altered the catchment-to-lake conveyor of coarse particles (EM3; Chambers, 1978) under higher flows. This illustrates the scale and non-linear effects of anthropogenic landscape alteration.

The second half of the 20th century and start of the 21st century features frequent flooding. Much of this interval experienced negative wNAO conditions but that cannot fully explain the trend. Sediment accumulation rates (SAR) were also higher at this time (Figure

730 7B), which could influence flood preservation potential. We attribute the initial rise in SAR to
731 mechanised ore extraction in the CE 1930s and 1940s, following the similar rise in the CE
732 1860s. Since then, the most likely driver is sheep rearing given, today, virtually the whole
733 catchment is pasture. Data from adjacent catchments (Windermere and Loweswater) reveal
734 a steady rise in sheep stocking densities since the 1950s (et al., 2012; Bennion and
735 Winchester, 2010). Moreover, Van der Post et al. (1997) found a strong correlation between
736 stocking density and post-CE 1950 SAR at Blelham Tarn. Greater sediment availability could
737 mean the system preserves a sedimentary signal from lower-magnitude floods. Based on the
738 stratigraphic match presented in Figure 6, however, a Mann-Kendall test shows no trend ($p = 0.2$) in discharges that left an imprint in Brotherswater over the timescale of the longest river
739 0.2) in discharges that left an imprint in Brotherswater over the timescale of the longest river
740 flow series (CE 1962 – present; Eamont Bridge). This leaves two explanations: flooding in the
741 Eden catchment is more frequent than earlier centuries or lower SAR in the past meant fewer
742 deposits were preserved, presumably representing the largest floods. It follows that our
743 reconstruction is therefore a minimum estimate of late-Holocene flood frequency in northwest
744 Britain.

745 Human-induced modifications to the coupled sediment-hydrological regime clearly
746 impose severe challenges where refining return period calculations using palaeoflood data is
747 the objective. On the other hand, hazards posed by sedimentologically intense flooding have
748 serious management implications for floodplain development (Hudson et al., 2008) and
749 aquatic health (Jones et al., 2011). Greater loading of fine sediment has particularly harmful
750 effects on fish spawning grounds, for example (Kemp et al., 2011). Such risks to infrastructure
751 and ecosystems highlights the importance of establishing long time series of
752 geomorphologically impactful floods (Hooke, 2015).

753

754 ***6. Conclusion***

755 We have developed the longest lake-derived palaeoflood reconstruction for the UK, spanning
756 the last 1500 years. Although the homogeneous sediment matrix extracted from Brotherswater
757 precluded visual identification of discrete flood deposits, an outlier detection routine identified
758 a series of anomalously coarse laminations. That 31 of 33 coarse deposits lain down since
759 CE 1800 link stratigraphically to independent records of high flows in the River Eden
760 catchment strongly supports their interpretation as flood units. Although end-member
761 modelling reveals a consistent sedimentary signature, there is evidence the system can at
762 times be supply limited. As a result, event sequencing appears to mask the imprints of
763 hydrological floods where major events occur within two successive years. This means
764 Brotherswater preserves a signal of sedimentologically intense floods—i.e., those causing

765 greatest geomorphic change—rather than capturing every high flow. Historically augmented
766 flood frequency analysis is likely, therefore, to produce a conservative estimate.
767 Our late-Holocene palaeoflood reconstruction reveals nine multi-decadal periods of
768 more frequent flooding (CE 510-630, 890-960, 990-1080, 1470-1560, 1590-1620, 1650-1710,
769 1740-1770, 1830-1890 and 1920-2012). Flood-rich episodes are significantly associated with
770 negative winter NAO conditions and four coincide with solar minima, further evidence that
771 ocean-atmosphere connectivity over the North Atlantic generates the westerly storm systems
772 responsible for most winter flooding in northwest England and western and central Europe.
773 Weak correlations with other climatic drivers highlight the challenge of elucidating flood-
774 generating mechanisms.
775 Frequent flooding at Brotherswater also coincides with geochemical and
776 sedimentological evidence of increased catchment erosion. Regional palynological and
777 geomorphological evidence indicates human activity (woodland clearance, grazing pressure
778 and mining expansion) has accelerated hillslope runoff and the sediment conveyor in this
779 system. We ascribe the apparent steady increase in baseline flood frequency in part to human-
780 induced catchment erosion and we propose that destabilised hillslopes conditioned the
781 catchment to be more sensitive to climatically driven floods. Disentangling and quantifying the
782 respective roles of anthropogenic and climatic drivers poses a major challenge to palaeoflood
783 research and this study illustrates that a deep understanding of the sedimentary system is a
784 vital precursor. Simulating their effects on long-term catchment sediment flux using landscape
785 evolution models can help to address this task (e.g., Welsh et al., 2009). Future
786 reconstructions should also stipulate whether flood deposits reflect extremes in discharge or
787 changes in sediment availability. Our findings showcase a method for extracting palaeoflood
788 information from lakes in temperate regions with organic-rich sediment matrices, which have
789 been widely overlooked to date. Developing this dataset worldwide could transform hazard
790 assessments of geomorphological impactful floods and their threat to ecosystems and
791 infrastructure.
792
793 **Acknowledgements**
794 DNS acknowledges the support of a Graduate Bursary from the University of Liverpool and
795 Kinsey Fund. Natural England, The National Trust, the Lake District National Park Authority
796 and The Brotherswater Inn are thanked for their on-going support for research at
797 Brotherswater. This work was supported by the NERC Radiocarbon Facility NRCF010001
798 (allocation number 1706.0413) and in part supported by a NERC Urgency Grant to RCC
799 (NE/P000118/1). We acknowledge the National River Flow Archive and BADC for hydrological
800 and meteorological data and the BGS is thanked for access to the G-BASE dataset. KEW

gratefully acknowledges financial support from the Manchester Geographical Society to conduct fieldwork and ^{210}Pb dating. We are grateful for use of the NERC supported Itrax facility (BOSCORF, National Oceanography Centre, Southampton). The authors thank Jeff Warburton and John Boyle for critical comments on earlier drafts and two anonymous reviewers for valuable and constructive suggestions that greatly improved the manuscript.

References

S., BARKER, P., HAWORTH, E.Y., LEAVITT, P.R., MABERLY, S.C., PATES, J., 2012. Humans and climate as drivers of algal community change in Windermere since 1850. Freshw. Biol. 57, 260–277. https://doi.org/10.1111/j.1365-2427.2011.02689.x

Amann, B., Szidat, S., Grosjean, M., 2015. A millennial-long record of warm season precipitation and flood frequency for the North-western Alps inferred from varved lake sediments: implications for the future. Quat. Sci. Rev. 115, 89–100. https://doi.org/10.1016/j.quascirev.2015.03.002

Appleby, P.G., Nolan, P.J., Gifford, D.W., Godfrey, M.J., Oldfield, F., Anderson, N.J., Batterbee, R.W., 1986. 210Pb dating by low background gamma counting. Hydrobiologia 143, 21–27.

Arnaud, F., Poulenard, J., Giguet-covex, C., Wilhelm, B., Revillon, S., Jenny, J.P., Revel, M., Enters, D., Majard, M., Chapron, E., Vanniere, B., Sabater, P., 2016. Erosion under climate and human pressures : An alpine lake sediment perspective r o. Quat. Sci. Rev. 152, 1–18. https://doi.org/10.1016/j.quascirev.2016.09.018

Baker, A., C. Hellstrom, J., Kelly, B.F.J., Mariethoz, G., Trouet, V., 2015. A composite annual-resolution stalagmite record of North Atlantic climate over the last three millennia. Sci. Rep. 5, 10307. https://doi.org/10.1038/srep10307

Ballantyne, C.K., 2002. A general model of paraglacial landscape response. The Holocene 12, 371–376. https://doi.org/10.1191/0959683602hl553fa

Beierle, B.D., Lamoureux, S.F., Cockburn, J.M.H., Spooner, I., 2002. A new method for visualizing sediment particle size distributions. J. Paleolimnol. 27, 279–283.

Benito, G., Thorndycraft, V.R., Rico, M., Sánchez-Moya, Y., Sopeña, a., 2008. Palaeoflood and floodplain records from Spain: Evidence for long-term climate variability and environmental changes. Geomorphology 101, 68–77.

https://doi.org/10.1016/j.geomorph.2008.05.020

Bennion, H., Winchester, A., 2010. Linking historical land-use change with palaeolimnological records of nutrient changes in Loweswater, Cumbria. Loweswater Care Project Short Project Report.

Blaauw, M., Andrés Christen, J., 2011. Flexible Paleoclimate Age-Depth Models Using an Autoregressive Gamma Process. Bayesian Anal. 6, 457–474. https://doi.org/10.1214/11-BA618

Blöschl, G., Hall, J., Parajka, J., Perdigão, R.A.P., Merz, B., Arheimer, B., Aronica, G.T., Bilibashi, A., Bonacci, O., Borga, M., Čanjevac, I., Castellarin, A., Chirico, G.B., Claps, P., Fiala, K., Frolova, N., Gorbachova, L., Gül, A., Hannaford, J., Harrigan, S., Kireeva, M., Kiss, A., Kjeldsen, T.R., Kohnová, S., Koskela, J.J., Ledvinka, O., Macdonald, N., Mavrova-Guirguinova, M., Mediero, L., Merz, R., Molnar, P., Montanari, A., Murphy, C., Osuch, M., Ovcharuk, V., Radevski, I., Rogger, M., Salinas, J.L., Sauquet, E., Šraj, M., Szolgay, J., Viglione, A., Volpi, E., Wilson, D., Zaimi, K., Živković, N., 2017. Changing climate shifts timing of European floods. Science (80-.). 357, 588–590. https://doi.org/10.1126/science.aan2506

Bøe, A.-G., Dahl, S.O., Lie, Ø., Nesje, A., 2006. Holocene river floods in the upper Glomma catchment, southern Norway: a high-resolution multiproxy record from lacustrine sediments. The Holocene 16, 445–455. https://doi.org/10.1191/0959683606hl940rp

Boyle, J.F., 1995. A simple closure mechanism for a compact, large-diameter, gravity corer. J. Paleolimnol. 13, 85–87.

Boyle, J.F., Chiverrell, R.C., Schillereff, D.N., 2015. Approaches to water content correction and calibration for µXRF core scanning: comparing x-ray scatter with simple regression of elemental concentrations, in: Rothwell, R.G., Croudace, I.W. (Eds.), Developments in Palaeoenvironmental Research: Micro-XRF Studies of Sediment Cores. Springer, Dordrecht.

Burt, S., McCarthy, M., Kendon, M., Hannaford, J., 2016. Cumbrian floods, 5/6 December 2015. Weather 71, 36–37. https://doi.org/10.1002/wea.2704

Burt, T.P., Ferranti, E.J.S., 2012. Changing patterns of heavy rainfall in upland areas: A case study from northern England. Int. J. Climatol. 32, 518–532. https://doi.org/10.1002/joc.2287

Burt, T.P., Howden, N.J.K., 2013. North Atlantic Oscillation amplifies orographic precipitation and river flow in upland Britain. Water Resour. Res. 49, 3504–3515. https://doi.org/10.1002/wrcr.20297

Chambers, K.C., 1978. Source-sediment relationship in Cumbrian Lakes. University of Reading.

Charman, D.J., Blundell, A., Chiverrell, R.C., Hendon, D., Langdon, P.G., 2006. Compilation of non-annually resolved Holocene proxy climate records: stacked Holocene peatland palaeo-water table reconstructions from northern Britain. Quat. Sci. Rev. 25, 336–350. https://doi.org/10.1016/j.quascirev.2005.05.005

Chen, C., Liu, L.-M., 1993. Joint Estimation of Model Parameters and Outlier Effects in Time Series. J. Am. Stat. Assoc. 88, 284–297. https://doi.org/10.2307/2290724

Chiverrell, R.C., 2006. Past and future perspectives upon landscape instability in Cumbria, northwest England. Reg. Environ. Chang. 6, 101–114. https://doi.org/10.1007/s10113-005-0005-6

Chiverrell, R.C., Harvey, a. M., Foster, G.C., 2007. Hillslope gullying in the Solway Firth — Morecambe Bay region, Great Britain: Responses to human impact and/or climatic deterioration? Geomorphology 84, 317–343. https://doi.org/10.1016/j.geomorph.2005.12.014

Chiverrell, R.C., Harvey, a. M., Hunter (née Miller), S.Y., Millington, J., Richardson, N.J., 2008. Late Holocene environmental change in the Howgill Fells, Northwest England. Geomorphology 100, 41–69. https://doi.org/10.1016/j.geomorph.2007.04.036

Clark, R., Parker, A., Anderson, D., Wilson, P., 2007. Late Holocene debris cone development and vegetation and land-use history in the Pasture Beck valley, Lake District, NW England. Proc. Yorksh. Geol. Soc.

Cockburn, J.M.H., Lamoureux, S.F., 2008. Inflow and lake controls on short-term mass accumulation and sedimentary particle size in a High Arctic lake: implications for interpreting varved lacustrine sedimentary records. J. Paleolimnol. 40, 923–942. https://doi.org/10.1007/s10933-008-9207-5

Croudace, I.W., Rindby, A., Rothwell, R.G., 2006. ITRAX: description and evalutation of a new multi-function X-ray core scanner, in: Rothwell, R.G. (Ed.), New Techniques in Sediment Core Analysis. Geological Society of London Special Publications, pp. 51–63.

894 Czymzik, M., Brauer, A., Dulski, P., Plessen, B., Naumann, R., von Grafenstein, U.,
895 Scheffler, R., 2013. Orbital and solar forcing of shifts in Mid- to Late Holocene flood
896 intensity from varved sediments of pre-alpine Lake Ammersee (southern Germany).
897 Quat. Sci. Rev. 61, 96–110. https://doi.org/10.1016/j.quascirev.2012.11.010

898 Czymzik, M., Muscheler, R., Brauer, A., 2016. Solar modulation of flood frequency in central
899 Europe during spring and summer on interannual to multi-centennial timescales. Clim.
900 Past 12, 799–805. https://doi.org/10.5194/cp-12-799-2016

901 De Luca, P., Hillier, J.K., Wilby, R.L., Quinn, N.W., Harrigan, S., 2017. Extreme multi-basin
902 flooding linked with extra-tropical cyclones. Environ. Res. Lett. 12.
903 https://doi.org/10.1088/1748-9326/aa868e

904 Dearing, J.A., 1997. Sedimentary indicators of lake-level changes in the humid temperate
905 zone: a critical review. J. Paleolimnol. 18, 1–14.

906 Denniston, R.F., Luetscher, M., 2017. Speleothems as high-resolution paleo flood archives.
907 Quat. Sci. Rev. 170, 1–13. https://doi.org/10.1016/j.quascirev.2017.05.006

908 Dietze, E., Hartmann, K., Diekmann, B., IJmker, J., Lehmkuhl, F., Opitz, S., Stauch, G.,
909 Wünnemann, B., Borchers, A., 2012. An end-member algorithm for deciphering modern
910 detrital processes from lake sediments of Lake Donggi Cona, NE Tibetan Plateau,
911 China. Sediment. Geol. 243–244, 169–180.
912 https://doi.org/10.1016/j.sedgeo.2011.09.014

913 Eden, P., Burt, S., 2010. Extreme monthly rainfall: November 2009. Weather 65, 82–83.
914 https://doi.org/10.1002/wea.568

915 Edwards, K.J., Whittington, G., 2001. Lake sediments, erosion and landscape change during
916 the Holocene in Britain and Ireland. Catena 42, 143–173.
917 https://doi.org/10.1016/S0341-8162(00)00136-3

918 Environment Agency, 2006. Cumbria floods technical report: factual report on the
919 meteorology, hydrology and impacts of the January 2005 flooding in Cumbria.

920 Fielding, J.J., Kemp, A.E.S., Bull, J.M., Cotterill, C.J., Pearce, B., Avery, R.S., Langdon,
921 P.G., Croudace, I.W., 2018. Palaeoseismology from microfabric and geochemical
922 analysis of lacustrine sediments , Windermere , UK. J. Geol. Soc. London. 175, 903–
923 914.

924 Folk, R.L., 1966. A review of grain-size parameters. Sedimentology 6, 73–93.

925 Folk, R.L., Ward, W.C., 1957. Brazos River bar (Texas); A study in the significance of grain
926 size parameters. J. Sediment. Res. 27, 3–26.

927 Foulds, S. a., Macklin, M.G., 2016. A hydrogeomorphic assessment of twenty-first century
928 floods in the UK. Earth Surf. Process. Landforms 41, 256–270.
929 https://doi.org/10.1002/esp.3853

930 Fowler, H., Kilsby, C.G., 2002. Precipitation and the North Atlantic Oscillation. Int. J.
931 Climatol. 22, 843–866.

932 Giguet-Covex, C., Arnaud, F., Enters, D., Poulenard, J., Millet, L., Francus, P., David, F.,
933 Rey, P., Wilhelm, B., Delannoy, J., 2012. Frequency and intensity of high-altitude floods
934 over the last 3.5 ka in northwestern French Alps (Lake Anterne). Quat. Res. 77, 12–22.
935 https://doi.org/10.1016/j.yqres.2011.11.003

936 Gilli, A., Anselmetti, F.S., Glur, L., Wirth, S.B., 2013. Lake Sediments as Archives of
937 Recurrence Rates and Intensities of Past Flood Events, in: Schneuwly-Bollschweiler,
938 M., Stoffel, M., Rudolf-Miklau, F. (Eds.), Dating Torrential Processes on Fans and
939 Cones, Advances in Global Change Research. Springer Netherlands, Dordrecht, pp.
940 225–242. https://doi.org/10.1007/978-94-007-4336-6

941 Girardclos, S., Schmidt, O.T., Sturm, M., Ariztegui, D., Pugin, A., Anselmetti, F.S., 2007. The
942 1996 AD delta collapse and large turbidite in Lake Brienz. Mar. Geol. 241, 137–154.
943 https://doi.org/10.1016/j.margeo.2007.03.011

944 Gray, S.T., 2004. A tree-ring based reconstruction of the Atlantic Multidecadal Oscillation
945 since 1567 A.D. Geophys. Res. Lett. 31, L12205.
946 https://doi.org/10.1029/2004GL019932

947 Hannaford, J., 2015. Climate-driven changes in UK river flows: A review of the evidence.
948 Prog. Phys. Geogr. 39, 29–48. https://doi.org/10.1177/0309133314536755

949 Hannaford, J., Marsh, T.J., 2008. High-flow and flood trends in a network of undisturbed
950 catchments in the UK. Int. J. Climatol. 28, 1325–1338. https://doi.org/10.1002/joc

951 Hooke, J., 2006. Hydromorphological adjustment in meandering river systems and the role
952 of flood events. IAHS-AISH Publ. 127–135.

953 Hooke, J.M., 2015. Variations in flood magnitude-effect relations and the implications for
954 flood risk assessment and river management. Geomorphology In Press.

955 Hua, Q., 2009. Radiocarbon: A chronological tool for the recent past. Quat. Geochronol. 4,
956 378–390. https://doi.org/10.1016/j.quageo.2009.03.006

957 Hudson, P.F., Middelkoop, H., Stouthamer, E., 2008. Flood management along the Lower
958 Mississippi and Rhine Rivers (The Netherlands) and the continuum of geomorphic
959 adjustment. Geomorphology 101, 209–236.
960 https://doi.org/10.1016/j.geomorph.2008.07.001

961 Hydrology, I. of, 1999. Flood Estimation Handbook. Wallingford.

962 Jones, J., Murphy, J., Collins, A., Sear, D., Naden, P., Armitage, P.D., 2011. The impact of
963 fine sediment on macro-invertebrates. River Res. Appl. 25, 1800–1821.
964 https://doi.org/10.1002/rra

965 Jones, P.D., Jonsson, T., Wheeler, D., 1997. Extension to the North Atlantic oscillation using
966 early instrumental pressure observations from Gibraltar and south-west Iceland. Int. J.
967 Climatol. 17, 1433–1450. https://doi.org/10.1002/(SICI)1097-
968 0088(19971115)17:13<1433::AID-JOC203>3.0.CO;2-P

969 Kämpf, L., Brauer, A., Swierczynski, T., Czymzik, M., Mueller, P., Dulski, P., 2014.
970 Processes of flood-triggered detrital layer deposition in the varved Lake Mondsee
971 sediment record revealed by a dual calibration approach. J. Quat. Sci. 29, 475–486.
972 https://doi.org/10.1002/jqs.2721

973 Kemp, P., Sear, D., Collins, A., Naden, P., Jones, I., 2011. The impacts of fine sediment on
974 riverine fish. Hydrol. Process. 25, 1800–1821. https://doi.org/10.1002/hyp.7940

975 Kjeldsen, T.R., Macdonald, N., Lang, M., Mediero, L., Albuquerque, T., Bogdanowicz, E.,
976 Brázdil, R., Castellarin, a., David, V., Fleig, a., Gül, G.O., Kriauciuniene, J., Kohnová,
977 S., Merz, B., Nicholson, O., Roald, L. a., Salinas, J.L., Sarauskiene, D., Šraj, M.,
978 Strupczewski, W., Szolgay, J., Toumazis, a., Vanneuville, W., Veijalainen, N., Wilson,
979 D., 2014. Documentary evidence of past floods in Europe and their utility in flood
980 frequency estimation. J. Hydrol. 517, 963–973.
981 https://doi.org/10.1016/j.jhydrol.2014.06.038

982 Kjeldsen, T.R., Prosdocimi, I., 2018. Assessing the element of surprise of record-breaking
983 flood events. J. Flood Risk Manag. 11, S541–S553. https://doi.org/10.1111/jfr3.12260

Knight, J.R., Folland, C.K., Scaife, A. a., 2006. Climate impacts of the Atlantic Multidecadal Oscillation. Geophys. Res. Lett. 33, L17706. https://doi.org/10.1029/2006GL026242

Lam, D., Thompson, C., Croke, J., Sharma, A., Macklin, M., 2017. Reducing uncertainty with flood frequency analysis: The contribution of paleoflood and historical flood information. Water Resour. Res. 53, 2312–2327. https://doi.org/10.1002/2016WR019959

López-de-Lacalle, J., 2017. Package “tsoutliers.”

Macdonald, N., Sangster, H., 2017. High-magnitude flooding across Britain since AD 1750. Hydrol. Earth Syst. Sci. 21, 1631–1650. https://doi.org/10.5194/HESS-21-1631-2017

Magilligan, F.J., Phillips, J.D., James, L.A., Gomez, B., 1998. Geomorphic and Sedimentological Controls on the Effectiveness of an Extreme Flood. J. Geol. 106, 87–96. https://doi.org/10.1086/516009

Marsh, T., Kirby, C., Muchan, K., Barker, L., Henderson, E., Hannaford, J., 2016. The winter floods of 2015/2016 in the UK -a review, National Hydrological Monitoring Programme.

McDougall, D., 2013. Glaciation style and the geomorphological record: evidence for Younger Dryas glaciers in the eastern Lake District, northwest England. Quat. Sci. Rev. 73, 48–58. https://doi.org/10.1016/j.quascirev.2013.05.002

Meyers, P.A., Ishiwatari, R., 1993. Lacustrine organic geochemistry - an overview of indicators of organic matter sources and diagenesis in lake sediments. Org. Geochem. 20, 867–900.

Miller, J.D., Kjeldsen, T.R., Hannaford, J., Morris, D.G., 2013. A hydrological assessment of the November 2009 floods in Cumbria, UK. Hydrol. Res. 44, 180–197. https://doi.org/10.2166/nh.2012.076

Moreno, A., Valero-Garcés, B.L., González-Sampériz, P., Rico, M., 2008. Flood response to rainfall variability during the last 2000 years inferred from the Taravilla Lake record (Central Iberian Range, Spain). J. Paleolimnol. 40, 943–961. https://doi.org/10.1007/s10933-008-9209-3

Munoz, S.E., Giosan, L., Therrell, M.D., Remo, J.W.F., Shen, Z., Sullivan, R.M., Wiman, C., O’Donnell, M., Donnelly, J.P., 2018. Climatic control of Mississippi River flood hazard amplified by river engineering. Nature 556, 95–98. https://doi.org/10.1038/nature26145

1013 Neal, R., Fereday, D., Crocker, R., Comer, R.E., 2016. A flexible approach to defining
1014 weather patterns and their application in weather forecasting over Europe. Meteorol.
1015 Appl. 23, 389–400. https://doi.org/10.1002/met.1563

1016 Orr, H.G., Carling, P.A., 2006. Hydro-climatic and land use changes in the River Lune
1017 catchment, northwest England: implications for catchment management. River Resour.
1018 Appl. 22, 239–255.

1019 Osleger, D.A., Heyvaert, A.C., Stoner, J.S., Verosub, K.L., 2009. Lacustrine turbidites as
1020 indicators of Holocene storminess and climate: Lake Tahoe, California and Nevada. J.
1021 Paleolimnol. 42, 103–122. https://doi.org/10.1007/s10933-008-9265-8

1022 Osmond, C.B., Roksandic, Z., 1981. Oecologia 117–124.

1023 Otto, F.E.L., Van Der Wiel, K., Van Oldenborgh, G.J., Philip, S., Kew, S.F., Uhe, P., Cullen,
1024 H., 2018. Climate change increases the probability of heavy rains in Northern
1025 England/Southern Scotland like those of storm Desmond -a real-time event attribution
1026 revisited Climate change increases the probability of heavy rains in Northern
1027 England/Southern Scotlan. https://doi.org/10.1088/1748-9326/aa9663

1028 Parkes, B., Demeritt, D., 2016. Defining the hundred year flood: A Bayesian approach for
1029 using historic data to reduce uncertainty in flood frequency estimates. J. Hydrol. 540,
1030 1189–1208. https://doi.org/10.1016/j.jhydrol.2016.07.025

1031 Pattison, I., Lane, S.N., 2012. The relationship between Lamb weather types and long-term
1032 changes in flood frequency, River Eden, UK. Int. J. Climatol. 32, 1971–1989.
1033 https://doi.org/10.1002/joc.2415

1034 Pennington, W.T.G., 1991. Palaeolimnology in the English Lakes - some questions and
1035 answers over fifty years. Hydrobiologia 214, 9–24.

1036 Pennington, W.T.G., Lishman, J.P., 1984. The post-glacial sediments of Blelham Tarn:
1037 geochemistry and palaeoecology. Archaeol. Hydrobiol. Suppl. 69, 1–54.

1038 Proctor, C., Baker, A., Barnes, W., 2002. A three thousand year record of North Atlantic
1039 climate. Clim. Dyn. 19, 449–454. https://doi.org/10.1007/s00382-002-0236-x

1040 Reed, D.W., Robson, A.J., 1999. Statistical Procedures for Flood Frequency Estimation, in:
1041 Flood Estimation Handbook, Volume 3. Institute of Hydrology, Wallingford.

1042 Reimer, P.J., Bard, E., Bayliss, A., Beck, J.W., Blackwell, P.G., Bronk, C., Caitlin, R., Hai,
1043 E.B., Edwards, R.L., 2013. Intcal13 and Marine13 radiocarbon age calibration curves 0
1044 – 50,000 years cal BP. Radiocarbon 55, 1869–1887.

1045 Roberson, S., Weltje, G.J., 2014. Inter-instrument comparison of particle-size analysers.
1046 Sedimentology 61, 1157–1174. https://doi.org/10.1111/sed.12093

1047 Sambrook Smith, G.H., Best, J.L., Ashworth, P.J., Lane, S.N., Parker, N.O., Lunt, I. a.,
1048 Thomas, R.E., Simpson, C.J., 2010. Can we distinguish flood frequency and magnitude
1049 in the sedimentological record of rivers? Geology 38, 579–582.
1050 https://doi.org/10.1130/G30861.1

1051 Schillereff, D.N., Chiverrell, R.C., Macdonald, N., Hooke, J.M., 2016a. Hydrological
1052 thresholds and basin control over paleoflood records in lakes. Geology 44, 43–46.
1053 https://doi.org/10.1130/G37261.1

1054 Schillereff, D.N., Chiverrell, R.C., Macdonald, N., Hooke, J.M., 2014. Flood stratigraphies in
1055 lake sediments: A review. Earth-Science Rev. 135, 17–37.
1056 https://doi.org/10.1016/j.earscirev.2014.03.011

1057 Schillereff, D.N., Chiverrell, R.C., Macdonald, N., Hooke, J.M., Welsh, K.E., 2016b.
1058 Quantifying system disturbance and recovery from historical mining-derived metal
1059 contamination at Brotherswater, northwest England. J. Paleolimnol. 1–17.
1060 https://doi.org/10.1007/s10933-016-9907-1

1061 Semertzidou, P., Piliposian, G.T., Chiverrell, R.C., Appleby, P.G., 2018. Long-term stability
1062 of records of fallout radionuclides in the sediments of Brotherswater, Cumbria (UK). J.
1063 Paleolimnol. 7. https://doi.org/10.1007/s10933-018-0055-7

1064 Sibley, A., 2009. Analysis of extreme rainfall and flooding in Cumbria. Weather 65, 287–292.

1065 Smith, K., Tobin, G.A., 1979. Topics in Applied Geography: Human adjustment to the Flood
1066 Hazard. Longman, London.

1067 Spencer, P., Faulkner, D., Perkins, I., Lindsay, D., Dixon, G., Parkes, M., Lowe, A.,
1068 Asadullah, A., Hearn, K., Gaffney, L., Parkes, A., James, R., 2017. The floods of
1069 December 2015 in northern England: description of the events and possible
1070 implications for flood hydrology in the UK. Hydrol. Res. 48, 1–29.
1071 https://doi.org/10.2166/nh.2017.092

1072 Steinhilber, F., Beer, J., Fröhlich, C., 2009. Total solar irradiance during the Holocene.
1073 Geophys. Res. Lett. 36, 1–5. https://doi.org/10.1029/2009GL040142

1074 Stucchi, M., Rovida, A., Gomez Capera, A.A., Alexandre, P., Camelbeeck, T., Demircioglu,
1075 M.B., Gasperini, P., Kouskouna, V., Musson, R.M.W., Radulianm, M., Sesetyan, K.,
1076 Vilanova, S., Baumont, D., Bungum, H., Fäh, D., Lenhardt, W., Makropoulos, K., M.,
1077 M.S.J., Scotti, O., Živčić, M., Albini, P., Batllo, J., Papaioannou, C., Tatevossian, R.,
1078 Locati, M., Meletti, C., Viganò, D., Giardini, D., 2013. The SHARE European
1079 Earthquake Catalogue (SHEEC). J. Seismol. 17, 523–544.
1080 https://doi.org/10.1007/s10950-012-9335-2

1081 Sturm, M., Matter, A., 1978. Turbidites and varves in Lake Brienz (Switzerland): deposition
1082 of clastic detritus by density currents, in: Matter, A., Tucker, M. (Eds.), Modern and
1083 Ancient Lake Sediments. Blackwell Scientific Publications, Oxford, pp. 145–166.

1084 Team, R.C., 2018. R: A language and environment for statistical computing.

1085 Trouet, V., Esper, J., Graham, N.E., Baker, A., Scourse, J.D., Frank, D.C., 2009. Persistent
1086 positive North Atlantic oscillation mode dominated the Medieval Climate Anomaly.
1087 Science 324, 78–80. https://doi.org/10.1126/science.1166349

1088 Tyler, I., 1992. Greenside: A Tale of Lakeland Miners. Red Earth Publications, Cumbria.

1089 Van der Post, K., Oldfield, F., Haworth, E., Crooks, P.J.R., Appleby, P.G., 1997. A record of
1090 accelerated soil erosion in the recent sediments of Bleham Tarn in the English Lake
1091 District. J. Paleolimnol. 18, 103–120.

1092 Vasskog, K., Nesje, a., Storen, E.N., Waldmann, N., Chapron, E., Ariztegui, D., 2011. A
1093 Holocene record of snow-avalanche and flood activity reconstructed from a lacustrine
1094 sedimentary sequence in Oldevatnet, western Norway. The Holocene 21, 597–614.
1095 https://doi.org/10.1177/0959683610391316

1096 Wilby, R.L., O'Hare, G., Barnsley, N., 1997. The North Altantic Oscillation Index and British
1097 Isles climate variability. Weather 52, 266–276.

1098 Wild, C., Wells, C., Anderson, D., Boardman, J., Parker, A., 2001. Evidence for medieval
1099 clearance in the Seathwaite Valley, Cumbria. Trans. Cumberl. Westmorl. Antiq.
1100 Archaeol. Soc. 1, 54–68.

1101 Wilhelm, B., Arnaud, F., Sabatier, P., Crouzet, C., Brisset, E., Chaumillon, E., Disnar, J.-R.,

Guiter, F., Malet, E., Reyss, J.-L., Tachikawa, K., Bard, E., Delannoy, J.-J., 2012. 1400years of extreme precipitation patterns over the Mediterranean French Alps and possible forcing mechanisms. Quat. Res. 78, 1–12. https://doi.org/10.1016/j.yqres.2012.03.003

Wilhelm, B., Arnaud, F., Sabatier, P., Magand, O., Chapron, E., Courp, T., Tachikawa, K., Fanget, B., Malet, E., Pignol, C., Bard, E., Delannoy, J.J., 2013. Palaeoflood activity and climate change over the last 1400 years recorded by lake sediments in the north-west European Alps. J. Quat. Sci. 28, 189–199. https://doi.org/10.1002/jqs.2609

Wilhelm, B., Ballesteros Canovas, J.A., Corella Aznar, J.P., Kämpf, L., Swierczynski, T., Stoffel, M., Støren, E., Toonen, W., 2018a. Recent advances in paleoflood hydrology: From new archives to data compilation and analysis. Water Secur. 3, 1–8. https://doi.org/10.1016/J.WASEC.2018.07.001

Wilhelm, B., Ballesteros Cánovas, J.A., Macdonald, N., Toonen, W.H.J., Baker, V., Barriendos, M., Benito, G., Brauer, A., Corella, J.P., Denniston, R., Glaser, R., Ionita, M., Kahle, M., Liu, T., Luetscher, M., Macklin, M., Mudelsee, M., Munoz, S., Schulte, L., St. George, S., Stoffel, M., Wetter, O., 2018b. Interpreting historical, botanical, and geological evidence to aid preparations for future floods. Wiley Interdiscip. Rev. Water e1318. https://doi.org/10.1002/wat2.1318

Wilhelm, B., Nomade, J., Crouzet, C., Litty, C., Sabatier, P., Belle, S., Rolland, Y., Revel, M., Courboulex, F., Arnaud, F., Anselmetti, F.S., 2016. Quantified sensitivity of small lake sediments to record historic earthquakes: Implications for paleoseismology. J. Geophys. Res. Earth Surf. 121, 2–16. https://doi.org/10.1002/2015JF003602.Received

Winchester, A., 1987. Landscape and society in medieval Cumbria. John Donald, Edinburgh.

Wirth, S.B., Gilli, A., Simonneau, A., Ariztegui, D., Vannière, B., Glur, L., Chapron, E., Magny, M., Anselmetti, F.S., 2013a. A 2000 year long seasonal record of floods in the southern European Alps. Geophys. Res. Lett. 40, 4025–4029. https://doi.org/10.1002/grl.50741

Wirth, S.B., Glur, L., Gilli, A., Anselmetti, F.S., 2013b. Holocene flood frequency across the Central Alps – solar forcing and evidence for variations in North Atlantic atmospheric circulation. Quat. Sci. Rev. 80, 112–128. https://doi.org/10.1016/j.quascirev.2013.09.002

1133